



City Research Online

City, University of London Institutional Repository

Citation: Moslem, F., Masdari, M., Fedir, K. & Moslem, B. (2022). Experimental investigation into the aerodynamic and aeroacoustic performance of bioinspired small-scale propeller planforms. *Proceedings of the Institution of Mechanical Engineers, Part G: Journal of Aerospace Engineering*, 237(1), pp. 75-90. doi: 10.1177/09544100221091322

This is the accepted version of the paper.

This version of the publication may differ from the final published version.

Permanent repository link: <https://openaccess.city.ac.uk/id/eprint/33148/>

Link to published version: <https://doi.org/10.1177/09544100221091322>

Copyright: City Research Online aims to make research outputs of City, University of London available to a wider audience. Copyright and Moral Rights remain with the author(s) and/or copyright holders. URLs from City Research Online may be freely distributed and linked to.

Reuse: Copies of full items can be used for personal research or study, educational, or not-for-profit purposes without prior permission or charge. Provided that the authors, title and full bibliographic details are credited, a hyperlink and/or URL is given for the original metadata page and the content is not changed in any way.

City Research Online:

<http://openaccess.city.ac.uk/>

publications@city.ac.uk

1 **Experimental Investigation into the**
2 **Aerodynamic and Aeroacoustic**
3 **Performance of Bioinspired Small-Scale**
4 **Propeller Planforms**

5

6 **Foad Moslem**

7 Experimental Aerodynamic and Aeroacoustic Laboratory, Faculty of New Sciences and
8 Technologies, University of Tehran, North Kargar Street, Tehran, 14395-1561, Iran
9 E-mail: foad.moslem@ut.ac.ir

10

11 **Mehran Masdari¹**

12 Assistant Professor

13 Experimental Aerodynamic and Aeroacoustic Laboratory, Faculty of New Sciences and
14 Technologies, University of Tehran, North Kargar Street, Tehran, 14395-1561, Iran
15 E-mail: m.masdari@ut.ac.ir

16

17 **Kirchu Fedir**

18 Associate Professor

19 Aviation Engines Department, National Aviation University, Liubomyra Huzara Ave, Kyiv,
20 03058, Ukraine
21 E-mail: fkirchu@nau.edu.ua

22

23 **Behzad Moslem**

24 Faculty of Industrial Engineering, Islamic Azad University Science and Research Branch,
25 Tehran, Iran
26 E-mail: behzad.moslem@srbiau.ac.ir

¹ Corresponding author. m.masdari@ut.ac.ir

1 **Abstract**

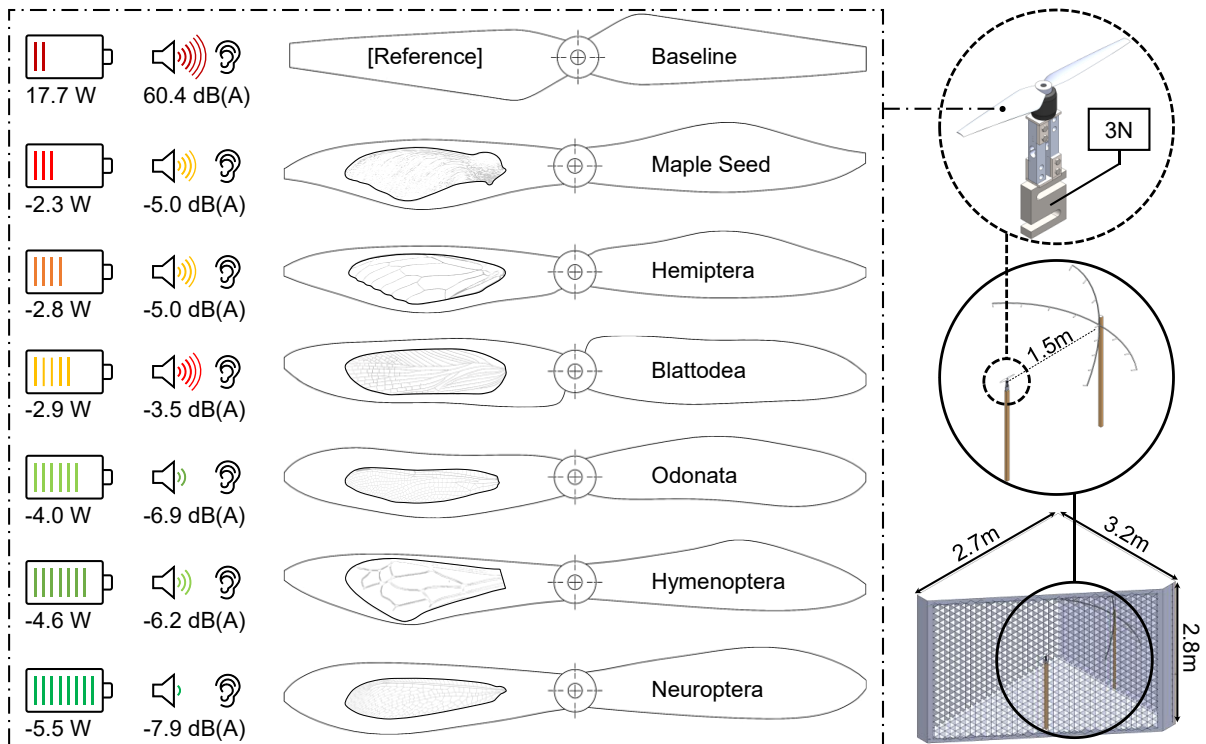
2 The multi-rotors have a limited operational period and generate too much noise, which
3 is insufficient for complex tasks and adversely affects humans' and animals' health.
4 Nevertheless, their market has become increasingly popular. Therefore, low-noise
5 products are more competitive, and aerodynamic and acoustic improvements are critical.
6 This investigation aims to design a small bioinspired propeller with the same power input
7 as a conventional propeller to achieve the same or better aerodynamic performance
8 while decreasing noise. Accordingly, an experimental investigated the impacts of
9 operation conditions and varied geometric parameters on six small propellers'
10 aeroacoustic performances with a unique planform shape inspired by five insects and one
11 plant, such as Blattodea, Hemiptera, Hymenoptera, Neuroptera, Odonata, and Maple Seed.
12 Each propeller was operated at eleven rotational speeds ranging from 3000 to 8000 RPM
13 with no freestream velocity for simulating hover conditions. Compared to the baseline
14 propeller, the results demonstrate that all bioinspired propellers produce more thrust for
15 the same power supply, reduce harmonic and broadband noise, and provide a better
16 noise level. Also, their rotational speed is lower and their figure of merit is higher than
17 the baseline propeller at hover flight with 3N thrust. They all outperform the baseline
18 propeller in terms of hover efficiency at all thrust values considered. Besides, the
19 Neuroptera propeller is more efficient than other propellers, and decreasing 5.5W of
20 power and reducing 7.9 dBA at hover flight with 3N thrust and 1.5 meters distance,
21 compared to the baseline propeller.

22

23 **Keywords:**

24 Aeroacoustics, Aerodynamic Performance, Propeller, Insect Bioinspiration, Planform

Graphical Abstract



NOMENCLATURE

A	Propeller disk area (m^2)	p_{ref}	Reference pressure, 2×10^{-5} Pa
C_Q	Coefficient of torque	Q	Torque (N. m)
C_T	Coefficient of thrust	R	Propeller radius (m)
dB	Decibel	SPL_A	A-weighted sound pressure level
$dB(A)$	A-weighted decibel	RPM	Revolutions per minute
FoM	Figure of merit	$sUAS$	Small Unmanned Aerial Systems
$OASPL$	Overall A-weighted sound pressure level	T	Thrust (N)
P_m	Mechanical power	$UASs$	Unmanned Aerial Systems
PL	Power loading	ρ	Flow density (kg/m^3)
p_A	Instantaneous sound pressure measured using the standard frequency weighting A	Ω	Propeller rotational speed (rev/sec)

1 **1. INTRODUCTION**

2 The Unmanned Aerial Systems (UASs) market has become increasingly popular for
3 commercial, recreational, and scientific research applications in recent years, due to their
4 small size, low-cost electronic devices, hovering and maneuvering ability, ability to
5 perform difficult or dangerous tasks, and user-friendly flight controllability. Various UAS
6 systems have been presented as a new means of transportation and delivery over
7 distances ranging from 1 to 300 km. Small Unmanned Aerial Systems (sUAS) have offered
8 promising solutions for various civilian applications, such as food and postal package
9 delivery, medical supplies delivery, surveillance, rescue operations, reaching hard-to-
10 reach areas, inspecting buildings, mapping construction, traffic control, aerial
11 photography, video recording, agriculture, and entertainment. Nowadays, multi-rotors
12 are the preferred sUAS platform, and their presence has been increased. Currently, multi-
13 rotors have an operational period of less than one hour, which is insufficient for complex
14 tasks. Besides, the noise generated from the operating multi-rotors is another essential
15 problem that can be limited to their use. Noise has adverse effects on humans' and
16 animals' health, such as fatigue, mental illness, cognitive dysfunction, aggression,
17 hormonal disorders, stress, stroke, heart attack, hypertension, diabetes, sleep disruption,
18 and hearing impairment [1]. Therefore, low-noise products are more competitive in the
19 market, and aerodynamic and acoustic improvements are critical to increasing
20 operational duration and lowering noise.

21 The two primary noise sources of multi-rotors are the propellers and the motors. The
22 propellers are the main source of lift generation and the predominant noise heard during
23 flight phases under normal conditions, so in comparison, the noise of the motors can be
24 ignored [2]. The propellers introduce complicated aerodynamic and aeroacoustic
25 interactions that understanding their characteristics is critical for more efficient and
26 quiet design. Figure 1 shows aerodynamic noise sources. Small propellers are operated
27 at lower Reynolds number regimes ($10^4 - 10^5$) and by decreasing the Reynolds number
28 in this range, the lift decreases, whereas the drag increases. Propellers only have a few
29 aerodynamic noise sources due to their size and Reynolds number regimes. A single
30 propeller blade's noise mechanisms contribute to two main classes: broadband noise and
31 harmonic noise. Harmonic noise includes thickness noise, loading noise, and blade-vortex
32 interactions. Thickness noise is caused by the fluid being displaced around the blade as it
33 turns and being directed towards the propeller plane. Loading noise is generated
34 predominantly above and below the propeller plane due to the surface's steady and
35 unsteady pressure loads. When the Mach number is less than one, the loading noise
36 outweighs the harmonic noise. However, blade-vortex interaction (BVI) noise is heard
37 when the previously generated tip vortices and entrance blade collision. Broadband noise
38 contains inflow turbulence and vortex noise. Inflow turbulence is present in broadband
39 noise, and vortex noise is produced by the interaction of the flow with various
40 components of the blade, such as the leading edge, trailing edge, blade-tip, or turbulent
41 flow in the wake.

1 There have been various noise reduction approaches to changing the design of the
2 propeller blade, but these techniques must have no profound impact on aerodynamic
3 performance and vehicle flight dynamics. Propeller noise studies, especially for larger
4 vehicles like helicopters, focus on harmonic and impulsive noise sources. However,
5 isolated small-scale propellers suffer from a different type of noise [3]. Tonal noise in the
6 low to mid-frequency region dominates isolated small-scale propellers, as it does full-
7 scale propellers [4]. Broadband noise is substantial for small propellers at higher
8 frequencies [5], [6]. In recent years, some experimental and numerical research has been
9 done to understand and improve the aerodynamic performance and aeroacoustic
10 signatures of small propellers in different flight modes and conditions, such as hover
11 flight, forward flight, and flight in harsh environments. Hovering quadrotors' noise
12 signatures can be considerably decreased by replacing them with customized propellers.
13 Zawodny and Boyd [7] studied hover acoustic measurements of isolated small propeller-
14 airframe interactions. According to the analysis, under certain propeller tip clearance
15 circumstances, the presence of the airframe surfaces might cause noise levels similar to
16 or larger than the propeller blade surfaces. Whelchel, Alexander, and Intaratep [8]
17 experimentally investigated the noise and thrust produced by four small propellers
18 operating at takeoff conditions and propeller-airframe interaction and compared them
19 with a DJI Matrice 600 Pro propeller. Brandt and Selig [9] tested 79 small propellers fitted
20 in the 9- to 11-in diameter that operate in the low Reynolds number range of 50,000 to
21 100,000 to quantify propeller efficiency. Propeller efficiencies range from a high of 0.65
22 (for an efficient propeller) to a low of 0.28 (for an efficient propeller). According to the
23 findings, appropriate propeller selection for UAVs can have a significant impact on
24 aircraft performance. Wisniewski *et al.* [10] analyzed thrust, sound pressure level (SPL),
25 and RPM data from a DJI standard propeller and three custom-designed propellers at 1.4
26 lbf thrust. They realized the noise signature of hovering quadcopters can be significantly
27 reduced by replacing them with custom-designed, wide chord multi-bladed propellers.
28 McKay and Kingan [11] observed that the minor variations in the small propeller's RPM
29 produced unsteady loading and thickness noise, and after that, blade passing frequency
30 tones started showing up. Zawodny and Haskin [12] performed a subsequent detailed
31 experimental investigation which showed how the relative importance of thickness and
32 loading noise changed with observer position and how interference between the two
33 noise sources could be important at specific locations. Andria *et al.* [13] presented a way
34 to improve small propeller performance. The modeling of the propeller's blades and hub,
35 followed by simulation to estimate thrust, was the first step in this procedure. Finally, the
36 thrust produced by different propellers was compared to better understand the changes
37 that may be made. The aeroacoustic fingerprints of two small propellers were studied
38 experimentally by Sinibaldi and Marino [14]. They observed that the improved propeller
39 produces significantly less noise than the standard propeller at lower thrust settings.

40 Active and passive flow control techniques can be utilized to increase propeller
41 performance and minimize noise. Active flow control methods are unviable for small
42 propellers. On the other hand, passive flow control approaches manipulate the boundary

1 layer without using any extra energy. Because flying animals have evolved over millions
2 of years to create efficient, high-performance wings, nature is an excellent source for
3 passive flow control approaches for designing bioinspired wings. Yang, Wang, *et al.* [15]
4 adopted an owl wing-inspired trailing-edge serrations for noise reduction of a small
5 propeller and compared its aerodynamic and acoustic performance with a baseline
6 propeller in the forward flight condition. Cambray *et al.* [16] investigated the noise
7 production process from small propellers as well as the influence of trailing-edge
8 serrations on noise reduction in their tests. Ning, Wlezien, and Hu [17] studied the noise
9 attenuation capability of three distinct bio-inspired saw-tooth serrations applied to the
10 baseline propeller to assess the serration's noise attenuation potential on a small
11 propeller. To achieve maximal noise reduction while preserving aerodynamic power,
12 Xiong, Nguyen, and Cramer [18] optimized an anti-phase alternating trailing-edge
13 pattern for propeller noise suppression. Yang, Liu, Hu, *et al.* [19] presented a small wavy
14 propeller and compared its aerodynamic and acoustic performance with a baseline
15 propeller. Hintz *et al.* [20] presented experimental research findings to determine the
16 influence of a bio-inspired blade planform on small-scale propeller thrust and energy
17 consumption. Ning and Hu [21] examined a small propeller's aerodynamic and
18 aeroacoustic properties with a novel planform shape inspired by the maple seed by
19 comparing it to a typical baseline propeller in hover flight. They showed that the
20 bioinspired propeller could provide equivalent thrust with constant power input while
21 emitting less noise.

22 The goal of this research is to create a small bioinspired propeller that has the same
23 power input as a conventional propeller and can achieve the same or better aerodynamic
24 performance while reducing noise. Nature appears to have done an incredible job of
25 designing insects' wings that are both practical and capable of sustained flight. Insects
26 have different species, fly slower than birds, and operate at low Reynolds number flows.
27 They take advantage of vortex patterns to provide the additional lift they require to fly
28 [22]. Several studies have connected flow separation and vortex generation to insect
29 flight's high lift aerodynamics [23]. The tip vortex adds significantly to the lift generated
30 by a flat plate with an aspect ratio and motion amplitudes equal to those seen in nature,
31 according to experimental studies [24]. Ning and Hu [21] showed that the majority of the
32 thrust for a rotary-wing is known to be created between 50% and 90% of the propeller
33 radius, and at Reynolds numbers ranging from 10,000 to 100,000, the lift to drag ratio
34 dramatically increases as the Reynolds number increases. As shown in Fig. 2, these
35 bioinspired wing planforms appear to be more compatible with the lift distribution,
36 where the largest chord length is in the high lift area. As a result, if these planform
37 configurations are used in the design, the propeller will operate at a better lift to drag
38 ratio. Accordingly, an experimental test is mainly used to study six small propellers'
39 aerodynamic and aeroacoustic performance with unique planform shapes inspired by
40 five insects and one plant, such as Blattodea, Hemiptera, Hymenoptera, Neuroptera,
41 Odonata, and Maple Seed. For the current investigation's comparison study, a typical
42 tapered small-scale propeller was used as the baseline propeller.

1

2 2. Experimental Setup

3 The experiments were performed in the Experimental Aerodynamics and
4 Aeroacoustics Research Laboratory's anechoic chamber at the University of Tehran. A
5 schematic of the facility is sketched out in Fig. 3. The inner dimensions of the anechoic
6 chamber from wedge tip to wedge tip are 3m long, 2.5m wide, and 2.56m tall with a low-
7 frequency cut-off of 100 Hz. To reduce noise contamination, the propeller noise and
8 loadings at the hover flight condition were measured using an external PC and DAQ.

9 Our experimental analysis compares the aeroacoustic features of seven propellers
10 with different planforms. We call the first one the baseline propeller and the others the
11 Blattodea, Hemiptera, Hymenoptera, Maple Seed, Neuroptera, and Odonata propellers,
12 respectively. The shape of the baseline propeller is derived from a two-bladed 9450
13 model for the DJI Phantom II that has a 9.4" diameter and a pitch of 5.0", which is a small-
14 scale commercial drone propeller used for video shooting and entertainment. The
15 Blattodea propeller's shape is inspired by a type of insect divided into approximately
16 4400 species of beetles and 3000 species of termites. The Hemiptera propeller's shape is
17 inspired by a type of insect with about 50 to 80 thousand species, including cicadas. Their
18 flying abilities are well developed for short distances and sporadically. The Hymenoptera
19 propeller's shape is inspired by one of the largest insect groups with more than 150,000
20 species, including bees. Their flight distance varies from small to large depending on the
21 species size, and they typically have two pairs of wings. The Maple Seed propeller's shape
22 is inspired by a thin, smooth wing with dry fibrous tissue attached to the nut of maple
23 tree seeds. Due to the grain weight relative to the whole structure, the seeds rotate like a
24 helicopter's propeller when they fall. The Neuroptera propeller's shape is inspired by a
25 type of insect with two pairs of membranous wings and consists of about 6,000 species.
26 Finally, The Odonata propeller's shape is inspired by a type of insect with two long,
27 transparent wings that move independently. They fly straight, and the flight muscles are
28 attached directly to the wings.

29 Based on Ning and Hu [21], the chord length from the largest chord on the planform to
30 the propeller's tip decreased linearly. It was calculated by $C_r = C_{tip}/r$, where C_r is the
31 chord length at the corresponding radius location, and r represents a non-dimensional
32 radial distance. The blade twisted 17.7 degrees at the largest chord on the planform to
33 4.7 degrees at the propeller's tip. Like Ning and Hu [21], due to a strength worry, we
34 reshaped every single profile with a doubled thickness E63 airfoil based on the camber
35 line and rescaled the diameter to 24cm fixed for both propellers, and our developed
36 propellers achieved 0.12 solidity like other ordinary small propellers. The schematic and
37 geometric details of all propellers are shown in Fig. 4. The propellers with a 0.1mm airfoil
38 trailing edge thickness were manufactured using the Umbreil3d 3D printer with a 100 μ m
39 resolution and a density of 20%, and were made by PLA material.

1 The experimental setup is shown in Fig. 3, which measures the thrust, torque, RPM,
2 and sound pressure level. The testing equipment was positioned on a lab stand 6.25D
3 above the surface such that the thrust was directed toward the chamber floor. When the
4 propeller is in hover mode, the entire rig experiences nearly no vibration. For the
5 measurement of the propeller thrust and torque, driven by an AIR 2213 electric brushless
6 Tiger Motor with 920 KV, a three-component balance (a 30kg force capacity AmCells S-
7 type and two 5kg force capacity YZC-133 loadcell) produced by the Experimental
8 Aerodynamics and Aeroacoustics Research Group was located directly below the motor.
9 An Agilent E3621A DC power supply provided power to the motor set at a constant 11.1
10 V for all tests. The propeller rotational speed was regulated using a T-Motor 20A AIR
11 electronic speed controller, which received time pulse signals from an Arduino Uno and
12 measured using a LUTRON DT-2268 tachometer. The T9545 propeller was tested to
13 validate the aerodynamic facility's accuracy, and the results were compared to its
14 datasheet, which showed the error was about 0.8%.

15 The microphone array is shown in Fig. 3. All acoustic measurements were made using
16 fifteen 1/2 inch free-field Bruel & Kjaer microphones type 4190 microphones. The
17 microphones were configured on two crossed C-shaped arrays at a 6.25D (1.5 meters)
18 radial distance from the center of the propeller and were positioned every 15° between
19 0° and 45° and every 7.5° between 0° and -30° on the roll-plane C-shape array
20 configuration and every 13° on the propeller plane from the common microphone. The
21 goal of this microphone array is to demonstrate noise reduction directivity and provide
22 more accurate results than a single microphone. Wind-screens covered the microphones,
23 and the frame was lined with absorbing material to reduce reflections. They were
24 individually calibrated using a B&K Type 4231 sound calibrator. The calibrator showed
25 ±0.2 dB calibration accuracy. The microphone's measurement uncertainty was ±1 dB up
26 to 20 kHz. Noise measurements were performed on all microphones, but only results for
27 microphone number five are reported for the sake of compactness. While acoustic
28 pressure was recorded for 15 seconds at a sampling rate of 48 kHz, only the last 5 seconds
29 of data was used to calculate the acoustic spectra. This time range was selected to
30 consider only the steady-state noise. The thrust, torque, and rotation rates were recorded
31 synchronously with the acoustic data. The balance data was collected for 5 seconds at a
32 sampling rate of 2000 Hz. The thrust, torque, RPM, and microphone data were recorded
33 using a LAN-XI DAQ data acquisition system and collected by an in-house developed data
34 acquisition and control. For each Fourier transform, the recorded acoustic data was
35 divided into time blocks of 1024 samples. Hanning windows were used, with a 50 percent
36 overlap.

37 While investigating the impacts of propeller operation conditions and varied
38 geometric parameters on aerodynamic loads and noise emissions, each propeller was
39 operated at eleven rotational speeds ranging from 3000 rpm to 8000 rpm in 500 rpm
40 increments. This rotation rate represents the typical RPM for small drones. Also, the
41 freestream velocity was 0 m/s because the propeller was operated at a simulated hover

1 condition. Representative values of local chord-based Reynolds and Mach numbers are
2 displayed in Table 1.

3 Before testing in place, the load cells were calibrated by applying known weights to
4 provide steady thrust and torque loads along the axis of each load cell, which covers the
5 range of propeller loadings, and the calibration was verified before each set of tests. The
6 thrust and torque measurement uncertainties were obtained at about 0.29% and 0.15%
7 of the full range. The repeatability of 20 measurements on the baseline model at 3000,
8 5500, and 8000 RPM was used to calculate the uncertainty of the microphone data. The
9 uncertainties for the total noise's overall A-weighted sound pressure level (OASPL) were
10 obtained at about 0.1 dB and 0.9 dB, respectively. The rotational speed uncertainty is 5
11 RPM, which can be ignored.

12

13 3. Results and Discussion

14 This section presents and discusses the contribution of a bioinspired planform to
15 modifying small propeller aerodynamic efficiency and acoustic signature in three parts.
16 In the first part, experimental aerodynamic performance is presented, and efficiency is
17 studied, in the second part, the experimental acoustic signature is investigated and noise
18 reduction is discussed, and in the last part aeroacoustic results compared to the T9545
19 propeller.

20

21 3.1. Aerodynamic Performance Results

22 The payload and endurance duration of multi-rotors are determined by aerodynamic
23 performance. To characterize the designed propellers' performance, the coefficient of
24 thrust (C_T), coefficient of torque (C_Q), mechanical power (P_m), and figure of merit (FoM)
25 have been calculated, as shown in Equations (1), (2), (3), and (4) respectively, where ρ is
26 flow density (kg/m^3), A is the propeller disk area (m^2), Ω is propeller rotational speed
27 (rev/sec), R is propeller radius (m), T is thrust (N), and Q is torque ($N.m$). Also, the
28 parameter of power loading (PL) is defined as the available thrust for a given power in
29 order to measure the efficiency of the rotors and is demonstrated by Equation (5). We
30 utilize both dimensional and non-dimensional data in propeller comparison, and there is
31 no obligation to use just non-dimensional data. Furthermore, the sound pressure level is
32 affected by the propeller's dimensional loading.

$$C_T = \frac{T}{\rho A \Omega^2 R^2} \quad (1)$$

$$C_Q = \frac{Q}{\rho A \Omega^2 R^3} \quad (2)$$

$$P_m = Q \cdot \left(2\pi \cdot \frac{RPM}{60}\right) \quad (3)$$

$$F_oM = \frac{C_T^{3/2} / \sqrt{2}}{C_Q} \quad (4)$$

$$PL = T/P \quad (5)$$

1

2 Figure 5 and 6 presents the comparative aerodynamic results. When the rotational
3 speed increase from 3000 RPM to 8000 RPM, the time-averaged thrust increase for the
4 baseline propeller from 0.51N to 3.82N, for the Blattodea propeller from 0.72N to 5.17N,
5 for Hemiptera propeller from 0.85N to 4.86N, for Hymenoptera propeller from 1.02N to
6 5.77N, for Maple Seed propeller from 0.74N to 5.04N, for Neuroptera propeller from
7 1.11N to 7.03N, and for Odonata propeller from 0.83N to 6.01N.

8 Also, when the rotational speed increase from 3000 RPM to 8000 RPM, the power
9 loading of the baseline increase from 0.07 N/W to 0.19 N/W, the Blattodea increase from
10 0.10 N/W to 0.26 N/W, the Hemiptera increase from 0.11 N/W to 0.24 N/W, the
11 Hymenoptera increase from 0.14 N/W to 0.29 N/W, the Maple Seed increase from 0.10
12 N/W to 0.25 N/W, the Neuroptera increase from 0.15 N/W to 0.35 N/W, and the Odonata
13 increase from 0.11 N/W to 0.30 N/W. Therefore, the power loading of the bioinspired-
14 planform propellers in all RPM and thrust ranges are higher than the baseline propeller.

15 At hover flight with 3N thrust, the rotational speed of the Neuroptera propeller is 4860
16 RPM, the Hymenoptera propeller is 5200 RPM, the Odonata propeller is 5460 RPM, the
17 Blattodea propeller is 5915 RPM, the Hemiptera propeller is 5925 RPM, the Maple Seed
18 propeller is 6120 RPM, and the baseline propeller is 7060 RPM. The results show that
19 Neuroptera is 36.6 %, Hymenoptera is 31.0 %, Odonata is 26.7 %, Blattodea is 19.1 %,
20 Hemiptera is 18.9 %, and Maple Seed is 15.7 % slower than the baseline propeller at the
21 same thrust. The drop in rotational speed shows that the thrust coefficient of the
22 bioinspired propellers is greater than that of the baseline propeller.

23 Further, at hover flight with 3N thrust, the required time-averaged power of the
24 Neuroptera propeller is 12.2W, the Hymenoptera propeller is 13W, the Odonata
25 propeller is 13.7W, the Blattodea and Hemiptera propellers are 14.8W, the Maple Seed
26 propeller is 15.3W, and the baseline propeller is 17.7W. The results indicate that the
27 Neuroptera propeller consumes 5.5W, the Hymenoptera propeller consumes 4.6W, the
28 Odonata propeller consumes 4.0W, the Blattodea and Hemiptera propellers consume
29 2.9W, and the Maple Seed propeller consumes 2.3W less power than the baseline
30 propeller at hover flight, and with a maximum power decrease of 31.0% in Neuroptera
31 propeller, 26.2% in Hymenoptera propeller, 22.6% in Odonata propeller, 16.2% in
32 Blattodea and Hemiptera propeller, and 13.3% in Maple Seed propeller, the bioinspired
33 propellers perform better than the baseline propeller. In conclusion, at hover flight with
34 3N thrust, the power loading of the Neuroptera propeller is 0.25 N/W, the Hymenoptera
35 propeller is 0.23 N/W, the Odonata propeller is 0.22 N/W, the Blattodea, Hemiptera, and
36 Maple Seed propellers are 0.20 N/W, and the baseline propeller is 0.17 N/W.

1 Furthermore, at hover flight with 3N thrust, the figure of merit of the Neuroptera
 2 propeller is 4.06, the Hymenoptera propeller is 3.79, the Odonata propeller is 3.52, the
 3 Hemiptera propeller is 3.34, the Blattodea propeller is 3.30, the Maple Seed propeller is
 4 3.20, and the baseline propeller is 2.79. At this thrust, the figure of merit of the
 5 Neuroptera propeller is about 45.5%, the Hymenoptera propeller is about 35.7%, the
 6 Odonata propeller is about 25.9%, the Hemiptera propeller is about 19.5%, the Blattodea
 7 propeller is about 18.1%, and the Maple Seed propeller is about 14.5% higher than the
 8 baseline propeller, which leads to less torque or more thrust.

9 The results demonstrate that the bioinspired propellers produce more thrust than the
 10 baseline propeller for the same power supply and generate less drag than the baseline
 11 propeller at hover flight with 3N thrust. At all thrust numbers evaluated, the bioinspired
 12 propellers exhibit greater hover efficiency than the baseline propeller. This trend can be
 13 attributed to the largest chord length closer to or at 50% to 90% of the spanwise, which
 14 is known as the lift booster area, and means the bioinspired planforms are beneficial in
 15 terms of aerodynamic efficiency. Compared to other bioinspired propellers, the
 16 Neuroptera propeller produced more thrust and showed higher hover efficiency.

17

18 3.2. Acoustic Signature Results

19 The aeroacoustic signature is characterized by an overall A-weighted sound pressure
 20 level (OASPL) at different frequencies and is calculated by Equations (6) and (7). Where
 21 SPL_A is A-weighted sound pressure level, $p_A(t)$ is the instantaneous sound pressure
 22 measured using the standard frequency weighting A, and p_{ref} is the reference pressure
 23 and equal to $2 \times 10^{-5} Pa$.

$$OASPL = 10 \log \sum_{i=1}^n 10^{\frac{SPL_A}{10}} \quad (6)$$

$$SPL_A = 20 \log \left(\frac{p_A(t)}{p_{ref}} \right) \quad (7)$$

24

25 As shown in Fig. 7, mechanical noise (no propeller) has little influence at low
 26 frequencies (2500 Hz) but grows significantly above that frequency. Clearly, motor noise
 27 plays a key role in the system's stress noise at low frequencies. Also, Fig. 7 shows that the
 28 bioinspired propellers can decrease harmonic and broadband noise more effectively than
 29 the baseline propeller at hover flight with 3N thrust. Harmonic noise is associated with
 30 blade passing frequency and consists of loading and thickness noise. When the Mach
 31 number is less than one, the loading noise takes precedence over the harmonic noise.
 32 However, it can decrease broadband noise more effectively than the baseline propeller at
 33 higher frequencies, due to the effect of the bioinspired planforms on the velocity gradient
 34 and pushing the wake vortices further from the trailing edge. This phenomenon reduces
 35 turbulent-boundary layer trailing edge noise and vortex shedding noise at the trailing

1 edge and decreases inter-mode interference involving modes from the propeller
2 apparent at higher frequencies. To better illustrate the differences in the graphs, the
3 original graphs are shown in transparent and the ninth degree polynomial is shown in
4 bold. This analysis helps to understand the noise characteristics of the bioinspired
5 planforms.

6 Figure 8 shows the OASPL directivity plot at hover flight with 3N thrust. As we move
7 up and down from microphone number five, the noise increases, which shows the
8 loading, broadband, and blade-vortex interaction noise have overcome the thickness
9 noise. The microphones on the roll plane show a distinct level of noise increasing and
10 more noise emitting at the top of the roll plane. There is a slight variation in rotor plane
11 microphone noises. As long as there is no interference from another rotor, the noise is
12 virtually constant throughout the rotor plane.

13 Figure 9 indicates changing OASPL values of microphone number five versus RPM and
14 thrust to evaluate the overall noise reduction. At microphone number five, when the
15 rotational speed increase from 3000 RPM to 8000 RPM, the OASPL of the baseline
16 propeller increase from 42.3 dBA to 64.4 dBA, the Blattodea propeller increase from 40.5
17 dBA to 63.4 dBA, the Hemiptera propeller increase from 40.5 dBA to 62.9 dBA, the
18 Hymenoptera propeller increase from 41.8 dBA to 64.5 dBA, the Maple Seed propeller
19 increase from 40.2 dBA to 62.4 dBA, the Neuroptera propeller increase from 40.6 dBA to
20 64.3 dBA, and the Odonata propeller increase from 40.9 dBA to 62.1 dBA. Due to the
21 difference in the generated thrust at the same RPM, the sound produced by the
22 bioinspired propellers is lower than the baseline propeller in all thrust ranges.

23 The OASPL at hover flight with 3N thrust for Neuroptera propeller is 52.5 dBA, for
24 Odonata propeller is 53.5 dBA, for Hymenoptera propeller is 54.2 dBA, for Hemiptera and
25 Maple Seed propellers are 55.4 dBA, for Blattodea propeller is 56.9 dBA, and for baseline
26 propeller is 60.4 dBA. Therefore, the results indicate that the Neuroptera propeller
27 generates 7.9 dBA, the Odonata propeller generates 6.9 dBA, the Hymenoptera propeller
28 generates 6.2 dBA, the Hemiptera and Maple Seed propeller generates 5 dBA, and the
29 Blattodea propeller generates 3.5 dBA less noise than the baseline propeller at
30 microphone number five and hover condition with 3N thrust.

31

32 **3.3. Aeroacoustic Results Compared to The T9545 Propeller**

33 Figure 10 presents the comparative aerodynamic and aeroacoustic performance
34 results. When the rotational speed increase from 3000 RPM to 8000 RPM, the time-
35 averaged thrust of the T9545 propeller increases from 0.79N to 5.63N, and the power
36 loading of the T9545 propeller increases from 0.11 N/W to 0.28 N/W. Therefore, the
37 power loading of the T9545 propeller in all RPM and thrust ranges is higher than the
38 baseline and lower than the Neuroptera, Hymenoptera, and Odonata propellers.

1 At hover flight with 3N thrust, the rotational speed of the T9545 propeller is 5777
2 RPM, which shows this propeller is 21.4Hz slower than the baseline propeller, and 15.3Hz
3 faster than the Neuroptera propeller, 9.6Hz faster than the Hymenoptera propeller, and
4 5.3Hz faster than the Odonata propeller at the same thrust.

5 Further, the required time-averaged power of the T9545 propeller at hover flight with
6 3N thrust is 14.5W. The results indicate that the T9545 propeller consumes 2.3W more
7 power than the Neuroptera propeller, 1.4W more power than the Hymenoptera
8 propeller, 0.8W more power than the Odonata propeller, and 0.3W less power than the
9 Blattodea and Hemiptera propeller, 0.8W less power than the Maple Seed propeller, 3.2W
10 less power than the baseline propeller at hover flight. With a maximum power decrease
11 of 18% at hover flight, the T9545 propeller performs better than the baseline propeller.
12 This propeller performs worse than Neuroptera, Hymenoptera, and Odonata propellers
13 with maximum power increase of 13%, 8.2%, and 4.6% at hover flight, respectively. In
14 conclusion, at hover flight with 3N thrust, the power loading of this propeller is 0.21 N/W.

15 Furthermore, the figure of merit of the T9545 propeller at hover flight with 3N thrust
16 is 3.05. The figure of merit of the T9545 propeller at this thrust is about 9.3% higher than
17 the baseline propeller. The figure of merit of the T9545 propeller is lower than the other
18 propellers.

19 The results demonstrate that the T9545 propeller produces more thrust than the
20 baseline, Blattodea, Maple Seed, and Hemiptera propellers and less thrust than the
21 Hymenoptera, Neuroptera, and Odonata propellers for the same power supply. Also,
22 T9545 propeller generates less drag than the baseline, Blattodea, Hemiptera, and Maple
23 Seed propellers and more drag than the Hymenoptera, Neuroptera, and Odonata
24 propellers at hover flight with 3N thrust.

25 The OASPL of the T9545 propeller at microphone number five increases from 38.3 dBA
26 to 62.5 dBA when the rotational speed increase from 3000 RPM to 8000 RPM. Also, the
27 OASPL at hover flight with 3N thrust for this propeller is 51.5 dBA. Therefore, the results
28 indicate that the T9545 propeller generates noise 1.0 dBA less than the Neuroptera
29 propeller, 2.0 dBA less than the Odonata propeller, 2.7 dBA less than the Hymenoptera
30 propeller, 3.8 dBA less than the Maple Seed propeller, 3.9 dBA less than the Hymenoptera
31 propeller, 5.4 dBA less than the Blattodea propeller, and 8.9 dBA less than the baseline
32 propeller at microphone number five and hover condition with 3N thrust.

33 Aeroacoustic results reveal that bioinspired propellers perform better than baseline
34 and T9545 propellers. It should be noted that the designed propellers have lower
35 manufacturing quality than the T9545 propeller. It is expected that by increasing the
36 manufacturing quality, the results of all propellers will improve, and the baseline
37 propeller shows results that are closer to those of the T9545 propeller.

38

39 4. Conclusions

1 An experimental investigated the impacts of operation conditions and varied
2 geometric parameters on six small propellers' aerodynamic and aeroacoustic
3 performance with a unique planform shape inspired by five insects and one plant, such
4 as Blattodea, Hemiptera, Hymenoptera, Neuroptera, Odonata, and Maple Seed. Each
5 propeller was operated at eleven rotational speeds ranging from 3000 to 8000 RPM with
6 no freestream velocity for simulating hover conditions. Finally, using force and sound, a
7 comparative experimental investigation into the aerodynamics and aeroacoustics
8 characteristics of the baseline and bioinspired propellers was undertaken in an anechoic
9 chamber. Compared to the baseline propeller, the results demonstrate that all
10 bioinspired propellers produce more thrust for the same power supply, reduce harmonic
11 and broadband noise, and provide a better noise level. This noise reduction can be
12 ascribed to the decreasing bioinspired propeller force variation. Also, their rotational
13 speed is lower and their figure of merit is higher than the baseline propeller at hover
14 flight with 3N thrust. They all outperform the baseline propeller in terms of hover
15 efficiency at all thrust values considered. Besides, the Neuroptera propeller is more
16 efficient than other propellers, decreasing 5.5W of power and reducing 7.9 dBA at hover
17 flight with 3N thrust and 1.5 meters distance, compared to the baseline propeller.

18 Future investigations will focus on some improvements. XFoil should be utilized to
19 guarantee that the best airfoil is chosen for each blade segment. Because noise generation
20 is affected by blade quality vibrations, a high-resolution (25 μ m) 3D printed using a rigid
21 material such as ABS plastic might offer accurate manufacturing precision. To increase
22 structural stiffness, the airfoil section from $r/R = 0.2$ should be smoothly integrated into
23 the hub. To ensure reliable printing output, the trailing edge airfoil utilized along the
24 propeller span (E63) should be thickened to 0.8 mm. The propeller should be connected
25 from the top to a profiled aluminum testing rig for the least amount of interference. To
26 decrease motor and test stand vibrations, a neoprene dampening material should be put
27 directly beneath the load cell. The sampling rate may be increased to 80 kHz. The
28 recording time may be increased by up to 20 seconds, and the data from the first 10
29 seconds could be utilized to compute acoustic spectra. It is necessary to investigate the
30 effects of recirculation within the anechoic chamber. To get a frequency resolution of
31 around 5 Hz, the number of FFT samples might be increased.

32 This study did not assess the influence of the existence of adjacent propellers and
33 forward flight, which makes them a great target for future investigations.
34 Furthermore, Smoke visualization, hotwire mapping, and PIV might be used to describe
35 the downwash flow of a propeller, among other methods.

36

37

38 **Declaration of Conflicting Interests**

39 The authors declare that there is no conflict of interest.

1 **References**

- 2 [1] Science for Environmental Policy, "FUTURE BRIEF: Noise Abatement Approaches,"
3 *EU Publ.*, no. 17, pp. 3–25, Apr. 2017, doi: 10.2779/016648.
- 4 [2] R. S. McKay and M. J. Kingan, "Multi-rotor unmanned aerial system noise:
5 Quantifying the motor's contribution," in *24th Acoustical Society of New Zealand*
6 *Conference*, 2018, no. 1.
- 7 [3] W. N. Alexander, J. Whelchel, N. Intaratep, and A. Trani, "Predicting community
8 noise of sUAS," in *25th AIAA/CEAS Aeroacoustics Conference, 2019*, 2019, doi:
9 10.2514/6.2019-2686.
- 10 [4] N. Intaratep, W. Nathan Alexander, W. J. Deveport, S. M. Grace, and A. Dropkin,
11 "Experimental study of quadcopter acoustics and performance at static thrust
12 conditions," in *22nd AIAA/CEAS Aeroacoustics Conference, 2016*, 2016, doi:
13 10.2514/6.2016-2873.
- 14 [5] N. S. Zawodny, D. D. Boyd, and C. L. Burley, "Acoustic characterization and
15 prediction of representative, small-scale rotary-wing unmanned aircraft system
16 components," in *Annual Forum Proceedings - AHS International*, 2016, vol. 1–2016,
17 pp. 34–48.
- 18 [6] S. E. Wright, "The acoustic spectrum of axial flow machines," *J. Sound Vib.*, vol. 45,
19 no. 2, pp. 165–223, 1976, doi: 10.1016/0022-460X(76)90596-4.
- 20 [7] N. S. Zawodny and D. D. Boyd, "Investigation of rotor–airframe interaction noise
21 associated with small-scale rotary-wing unmanned aircraft systems," *J. Am.*
22 *Helicopter Soc.*, vol. 65, no. 1, 2020, doi: 10.4050/JAHS.65.012007.
- 23 [8] J. Whelchel, W. N. Alexander, and N. Intaratep, "Propeller noise in confined anechoic
24 and open environments," in *AIAA Scitech 2020 Forum*, 2020, vol. 1 PartF, doi:
25 10.2514/6.2020-1252.
- 26 [9] J. Brandt and M. Selig, "Propeller Performance Data at Low Reynolds Numbers,"
27 2011, doi: 10.2514/6.2011-1255.
- 28 [10] C. F. Wisniewski, A. R. Byerley, K. W. Van Treuren, and A. Hays, "Experimentally
29 testing commercial and custom designed Quadcopter propeller static performance
30 and noise generation," in *23rd AIAA/CEAS Aeroacoustics Conference, 2017*, 2017,
31 doi: 10.2514/6.2017-3711.
- 32 [11] R. S. McKay and M. J. Kingan, "Multirotor unmanned aerial system propeller noise
33 caused by unsteady blade motion," in *25th AIAA/CEAS Aeroacoustics Conference,*
34 *2019*, 2019, doi: 10.2514/6.2019-2499.
- 35 [12] N. S. Zawodny and H. H. Haskin, "Small propeller and rotor testing capabilities of
36 the NASA langley low speed aeroacoustic wind tunnel," in *23rd AIAA/CEAS*
37 *Aeroacoustics Conference, 2017*, 2017, doi: 10.2514/6.2017-3709.
- 38 [13] G. Andria *et al.*, "Design and performance evaluation of drone propellers," in *5th*
39 *IEEE International Workshop on Metrology for AeroSpace, MetroAeroSpace 2018 -*
40 *Proceedings*, 2018, pp. 407–412, doi: 10.1109/MetroAeroSpace.2018.8453604.
- 41 [14] G. Sinibaldi and L. Marino, "Experimental analysis on the noise of propellers for

- 1 small UAV,” *Appl. Acoust.*, vol. 74, no. 1, pp. 79–88, 2013, doi:
2 10.1016/j.apacoust.2012.06.011.
- 3 [15] Y. Yang, Y. Wang, Y. Liu, H. Hu, and Z. Li, “Noise reduction and aerodynamics of
4 isolated multi-copter rotors with serrated trailing edges during forward flight,” *J.*
5 *Sound Vib.*, vol. 489, 2020, doi: 10.1016/j.jsv.2020.115688.
- 6 [16] A. Cambray, E. Pang, S. A. Showkat Ali, D. Rezgui, and M. Azarpeyvand,
7 “Investigation towards a better understanding of noise generation from UAV
8 propellers,” in *2018 AIAA/CEAS Aeroacoustics Conference*, 2018, doi:
9 10.2514/6.2018-3450.
- 10 [17] Z. Ning, R. Wlezien, and H. Hu, “An experimental study on small UAV propellers
11 with serrated trailing edges,” in *47th AIAA Fluid Dynamics Conference, 2017*, 2017,
12 doi: 10.2514/6.2017-3813.
- 13 [18] J. Xiong, N. Nguyen, and N. B. Cramer, “Acoustic optimization for anti-phase
14 asymmetric rotor,” in *AIAA Scitech 2020 Forum*, 2020, vol. 1 PartF, doi:
15 10.2514/6.2020-1496.
- 16 [19] Y. Yang *et al.*, “Experimental study on noise reduction of a wavy multi-copter rotor,”
17 *Appl. Acoust.*, vol. 165, 2020, doi: 10.1016/j.apacoust.2020.107311.
- 18 [20] C. Hintz, P. Khanbolouki, A. M. Perez, M. Tehrani, and S. V. Poroseva, “Experimental
19 study of the effects of bio-inspired blades and 3D printing on the performance of a
20 small propeller,” in *2018 Applied Aerodynamics Conference*, 2018, doi:
21 10.2514/6.2018-3645.
- 22 [21] Z. Ning and H. Hu, “An experimental study on the aerodynamic and aeroacoustic
23 performances of a bio-inspired UAV propeller,” in *35th AIAA Applied Aerodynamics*
24 *Conference, 2017*, 2017, doi: 10.2514/6.2017-3747.
- 25 [22] Z. J. Wang, “Two dimensional mechanism for insect hovering,” *Phys. Rev. Lett.*, vol.
26 85, no. 10, pp. 2216–2219, 2000, doi: 10.1103/PhysRevLett.85.2216.
- 27 [23] J. Young, S. M. Walker, R. J. Bomphrey, G. K. Taylor, and A. L. R. Thomas, “Details of
28 insect wing design and deformation enhance aerodynamic function and flight
29 efficiency,” *Science (80-.)*, vol. 325, no. 5947, pp. 1549–1552, 2009, doi:
30 10.1126/science.1175928.
- 31 [24] M. J. Ringuette, M. Milano, and M. Gharib, “Role of the tip vortex in the force
32 generation of low-aspect-ratio normal flat plates,” *J. Fluid Mech.*, vol. 581, pp. 453–
33 468, 2007, doi: 10.1017/S0022112007005976.

Figure Captions List

- Fig. 1 Aerodynamic noise sources
- Fig. 2 Baseline and bioinspired wing planforms and their maximum chord location
- Fig. 3 Schematic of the facilities and microphone array
- Fig. 4 Schematic and geometric details of bioinspired propellers compared to the baseline propeller
- Fig. 5 Aerodynamic performance results compared to the baseline propeller
- Fig. 6 Power loading results compared to the baseline propeller
- Fig. 7 Acoustic signature results compared to the baseline propeller
- Fig. 8 Bioinspired propellers noise directivity at hover flight with 3N thrust compared to the baseline propeller at microphone number five
- Fig. 9 Aeroacoustic performance results compared to the baseline propeller at microphone number five
- Fig. 10 Aerodynamic, Acoustic, and Aeroacoustic performance results of bioinspired propellers compared to the T9545 propeller at microphone number five

Table Caption List

- Table 1 Local chord-based Reynolds and Mach numbers of propellers

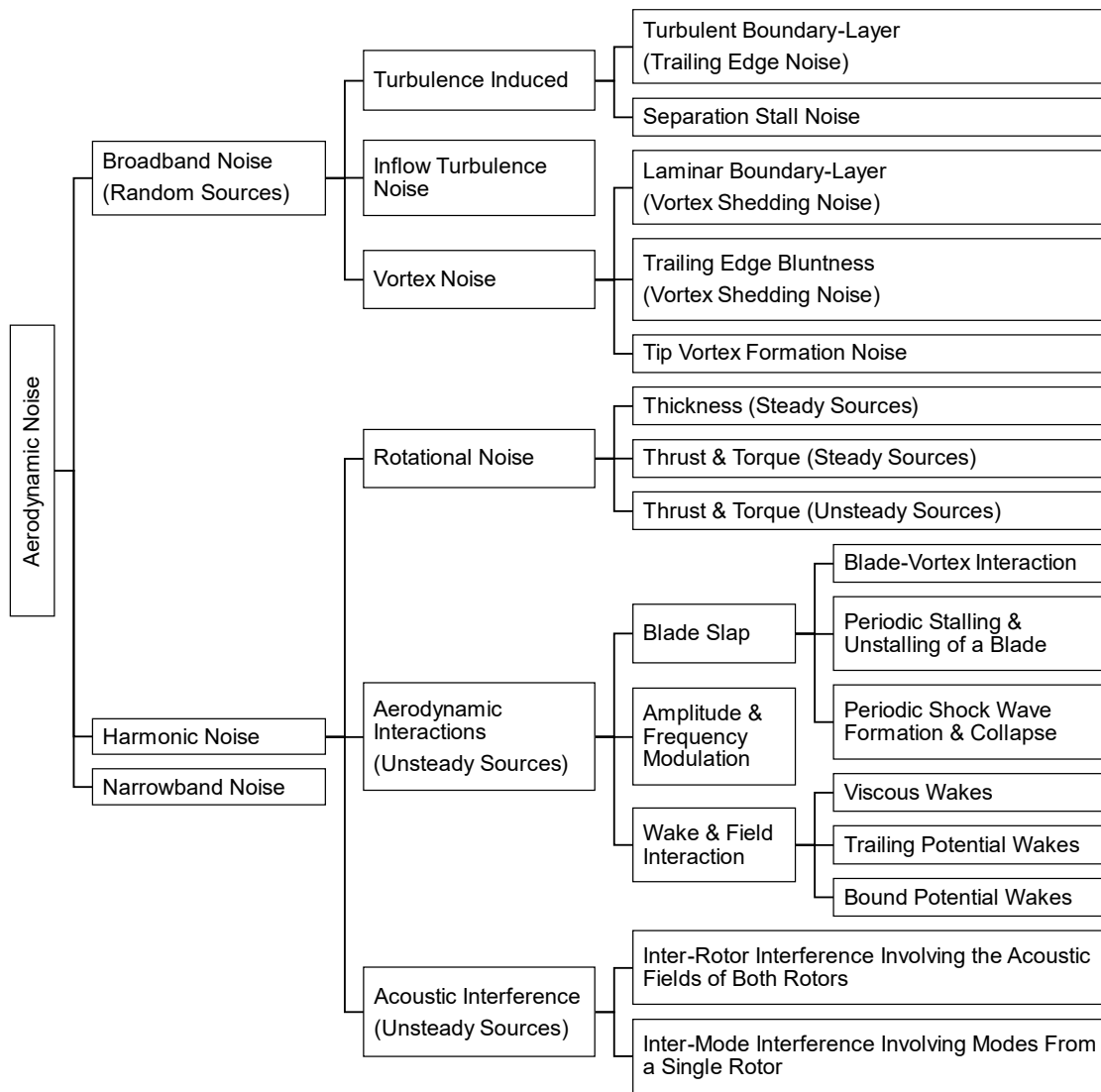


Fig. 1 Aerodynamic noise sources

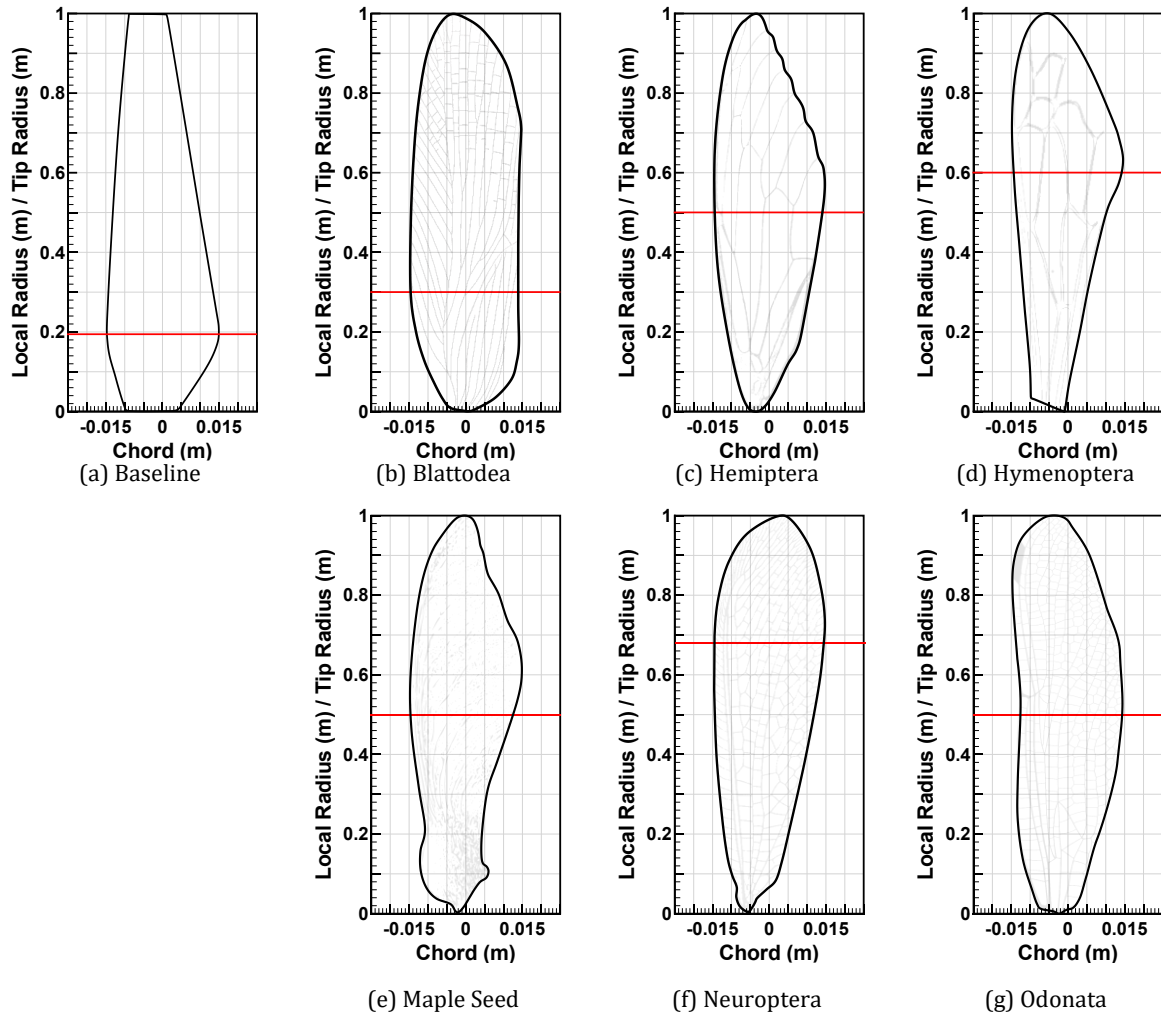


Fig. 2 Baseline and bioinspired wing planforms and their maximum chord location

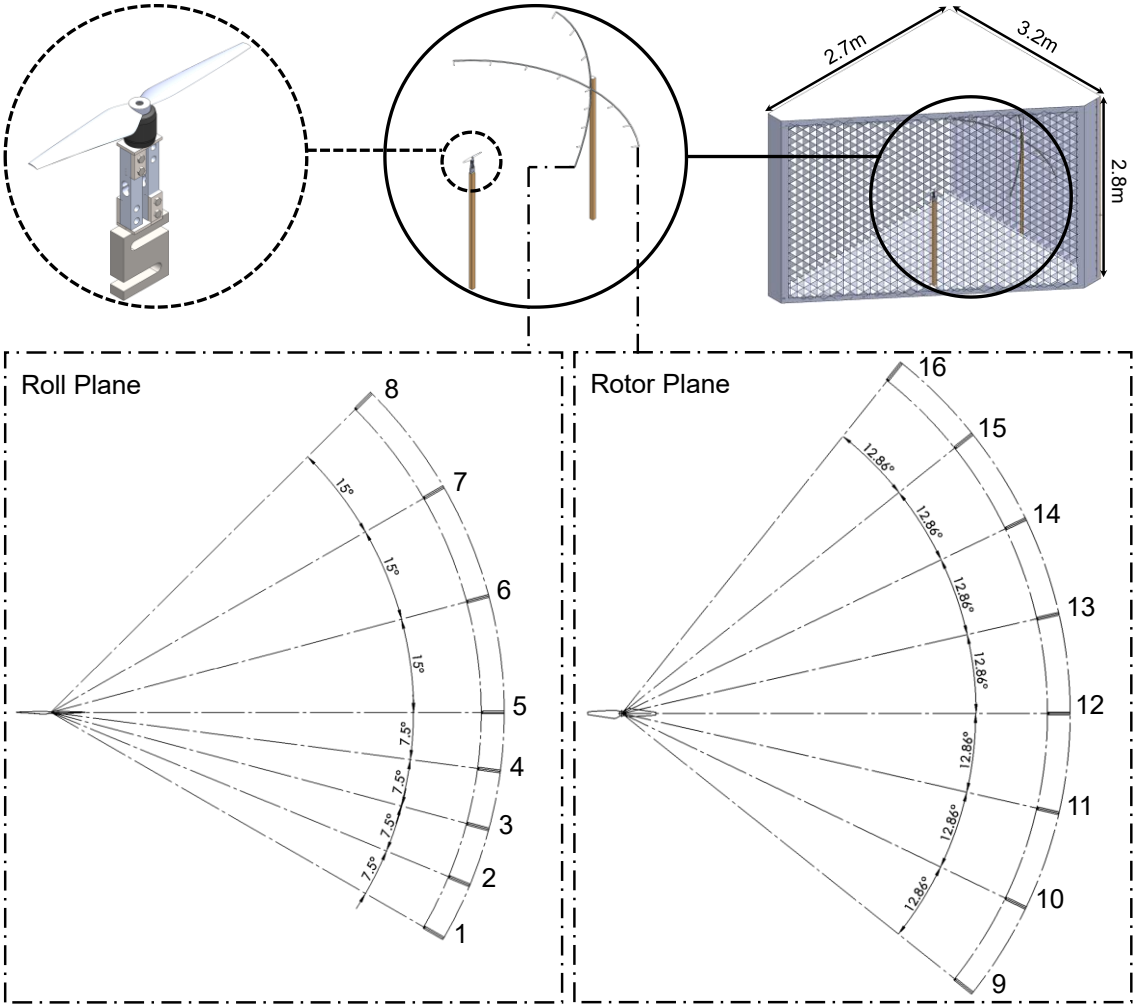
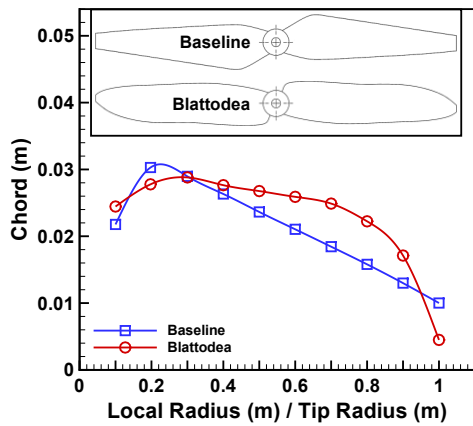
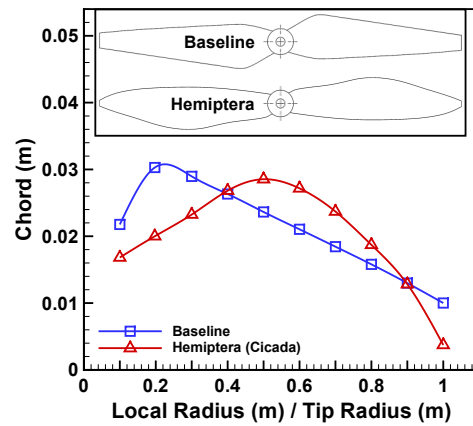


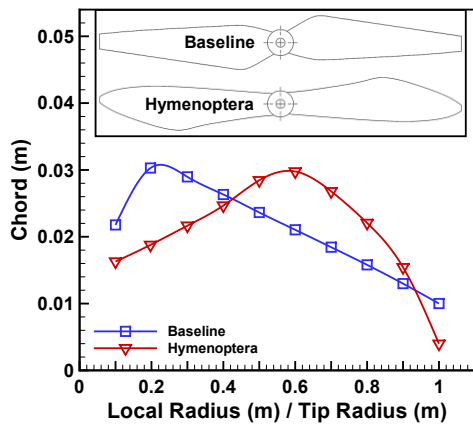
Fig. 3 Schematic of the facilities and microphone array



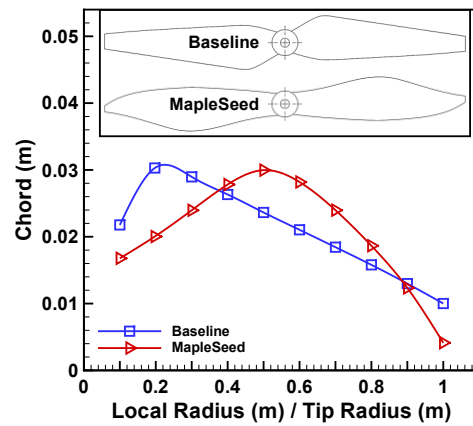
(a) Baseline and Blattodea



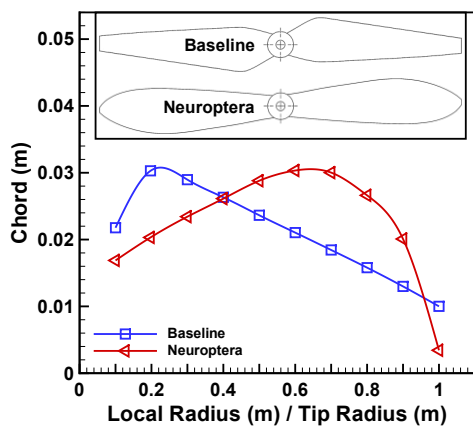
(b) Baseline and Hemiptera



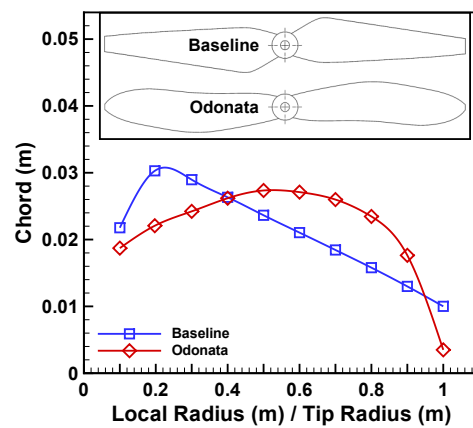
(c) Baseline and Hymenoptera



(d) Baseline and MapleSeed

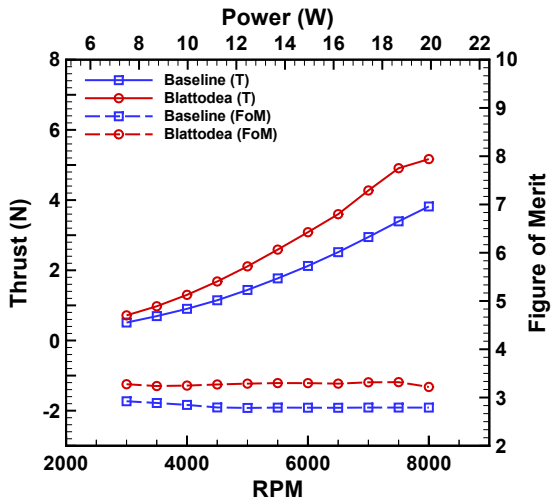


(e) Baseline and Neuroptera

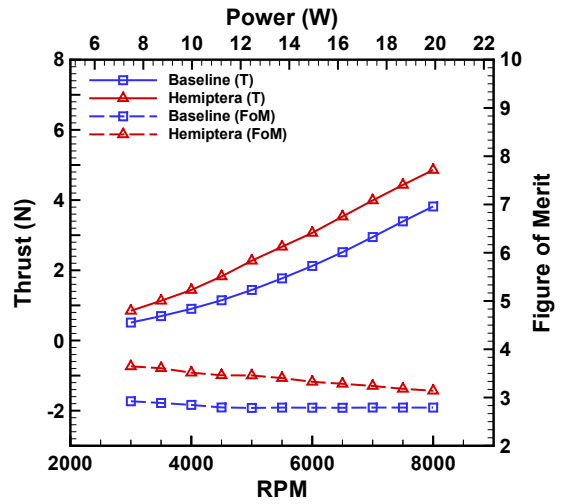


(f) Baseline and Odonata

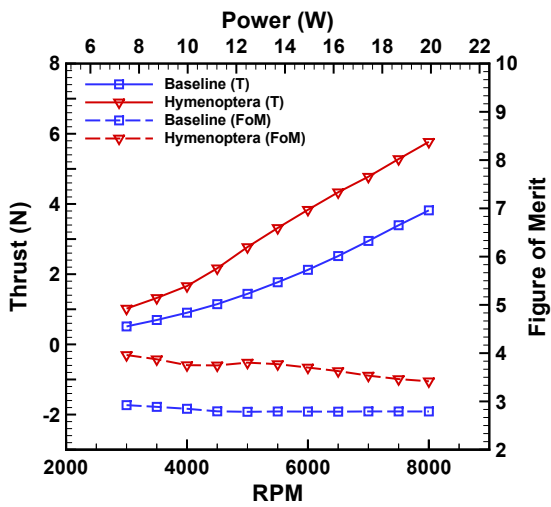
Fig. 4 Schematic and chord distribution of propellers compared to the baseline propeller



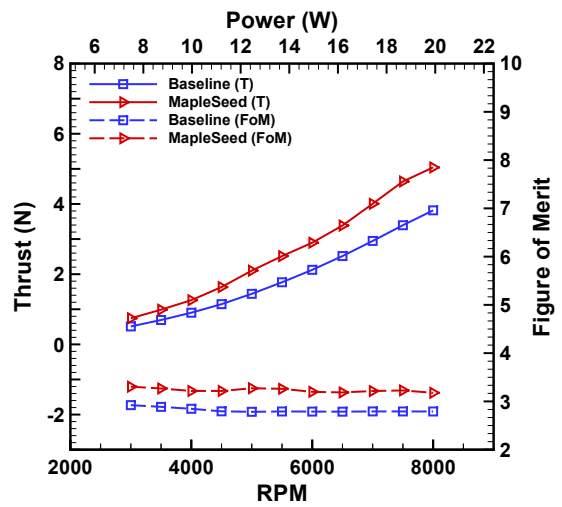
(a) Baseline and Blattodea



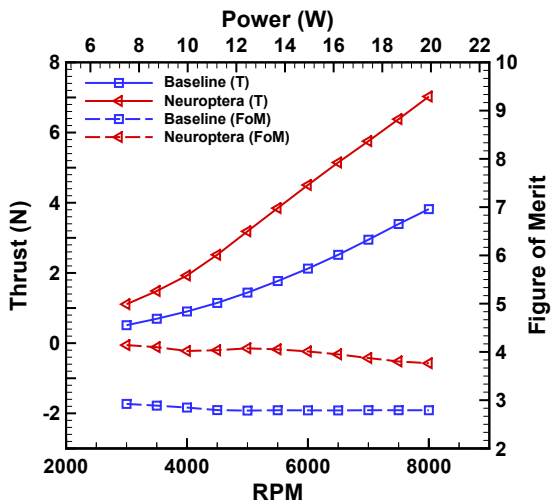
(b) Baseline and Hemiptera



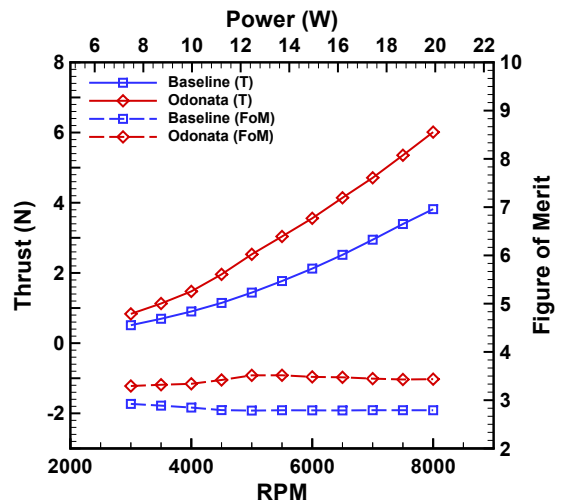
(c) Baseline and Hymenoptera



(d) Baseline and MapleSeed

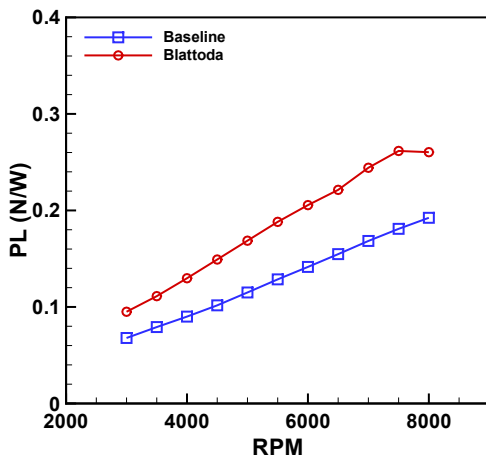


(e) Baseline and Neuroptera

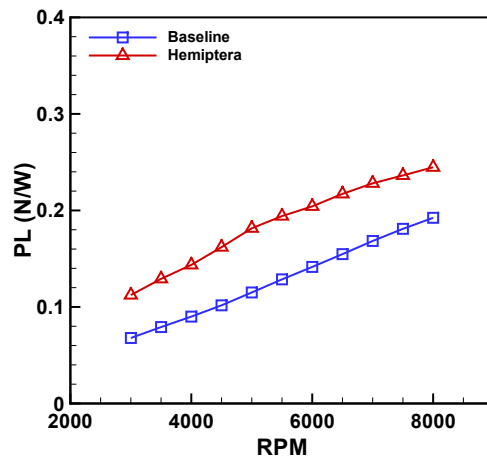


(f) Baseline and Odonata

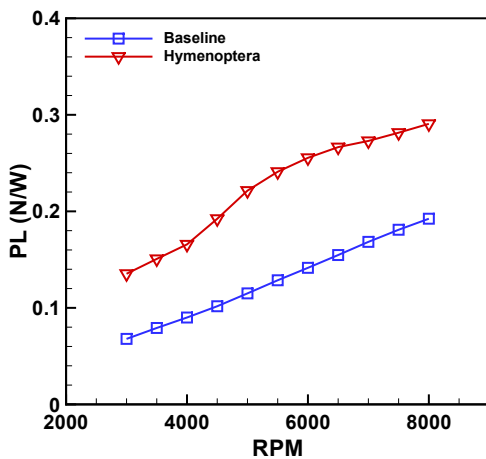
Fig. 5 Aerodynamic performance results compared to the baseline propeller



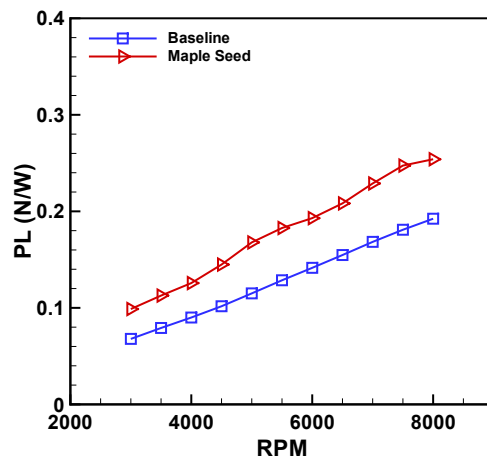
(a) Baseline and Blattodea



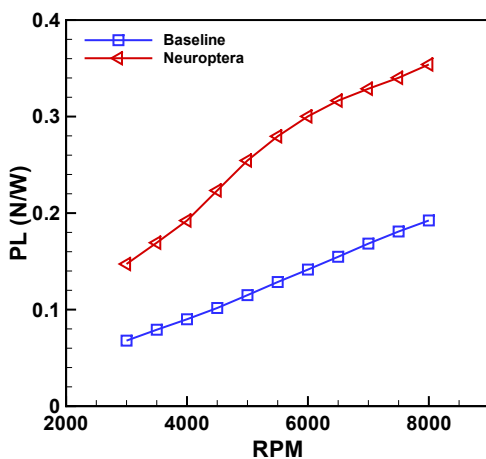
(b) Baseline and Hemiptera



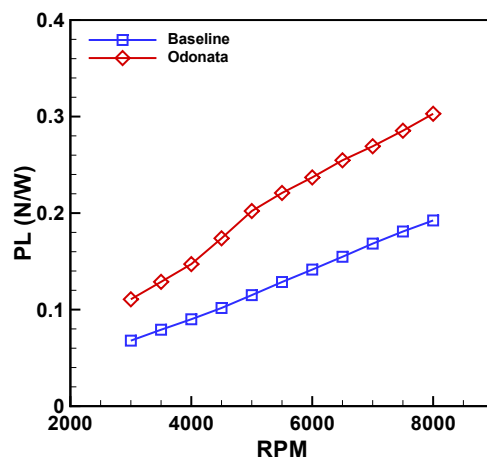
(c) Baseline and Hymenoptera



(d) Baseline and MapleSeed

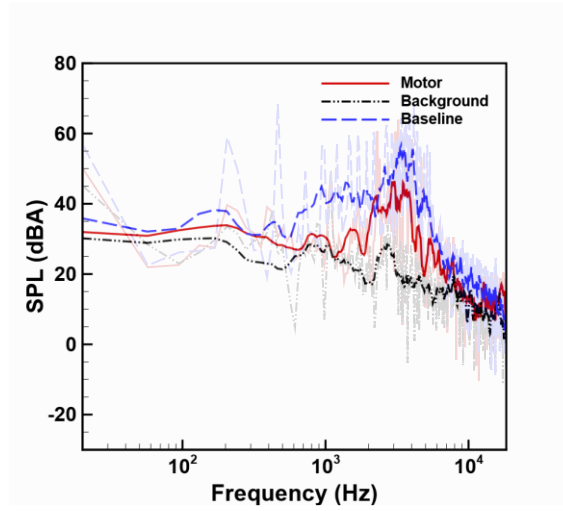


(e) Baseline and Neuroptera

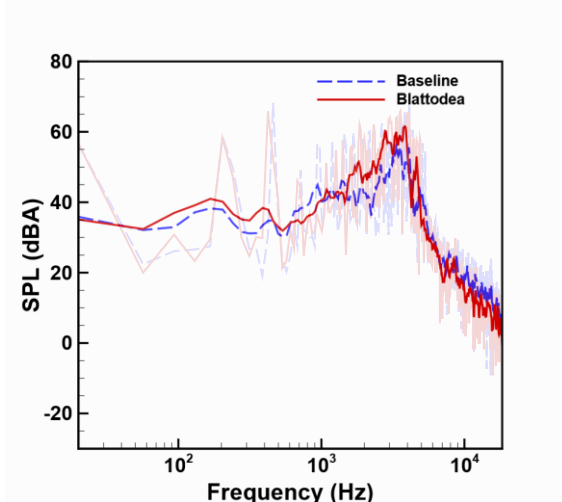


(f) Baseline and Odonata

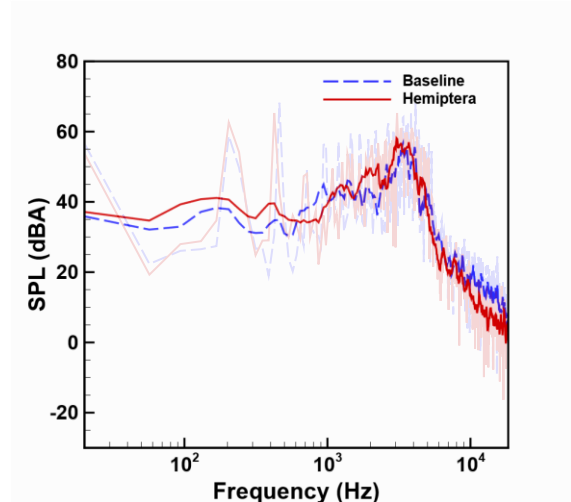
Fig. 6 Power loading results compared to the baseline propeller



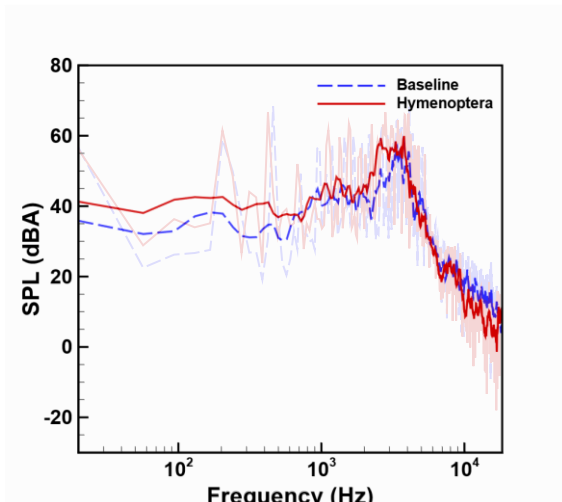
(a) Baseline, Background, and Motor



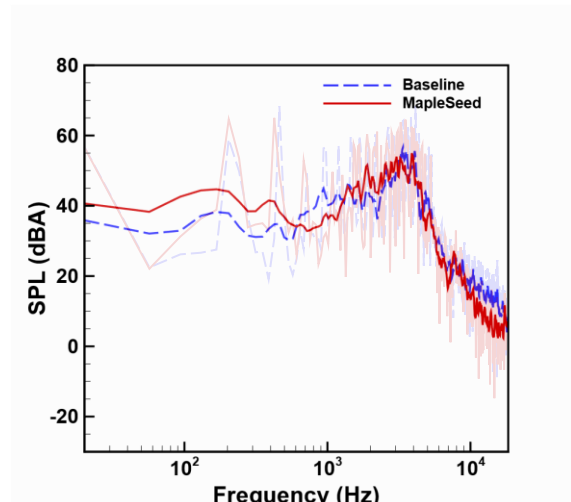
(b) Baseline and Blattodea



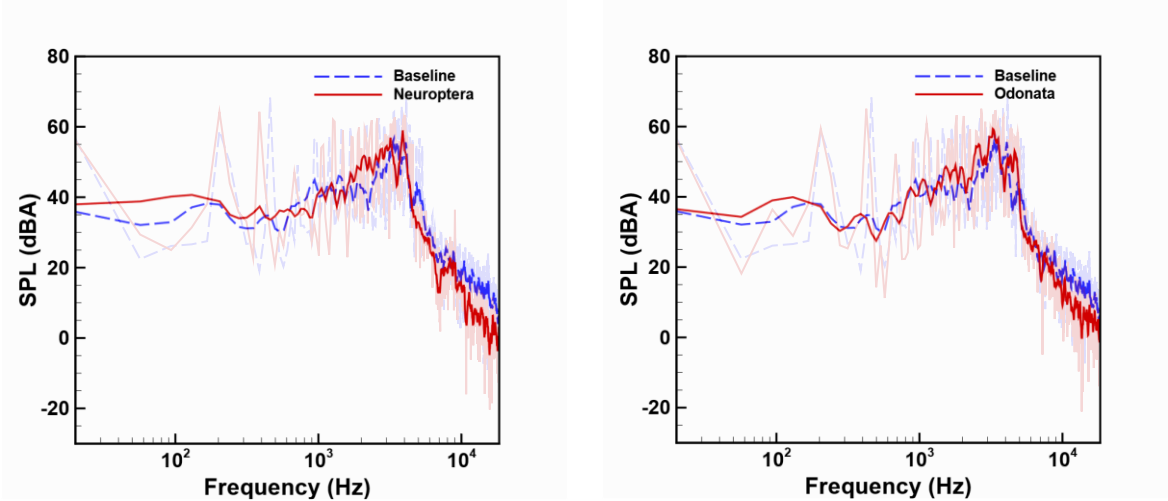
(c) Baseline and Hemiptera



(d) Baseline and Hymenoptera



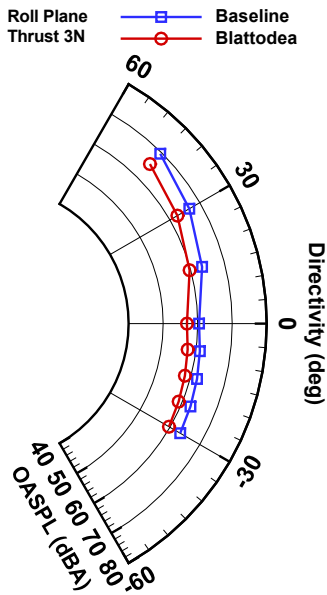
(e) Baseline and Maple Seed



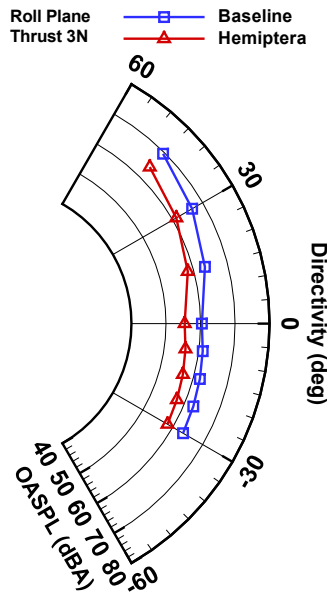
(f) Baseline and Neuroptera

(g) Baseline and Odonata

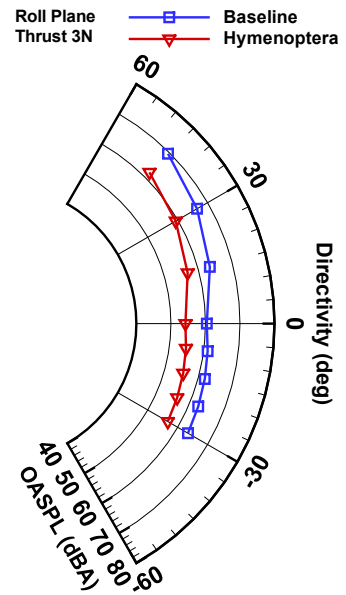
Fig. 7 Acoustic signature results compared to the baseline propeller at hover flight with 3N thrust (To better illustrate the differences in the graphs, the original graphs are shown in transparent and the ninth degree polynomial is shown in bold.)



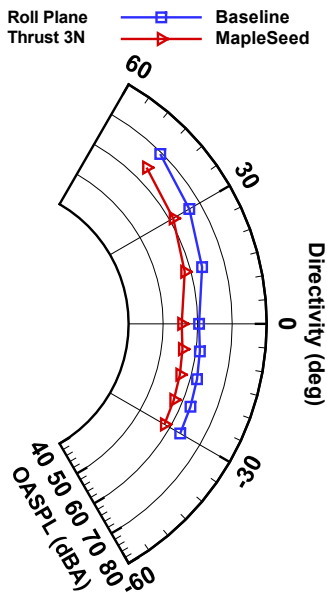
(a) Baseline and Blattodea roll plane directivity comparison



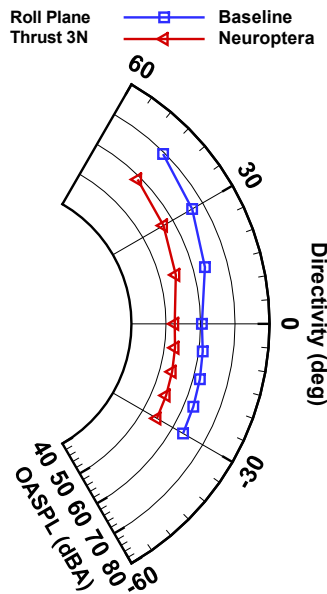
(b) Baseline and Hemiptera roll plane directivity comparison



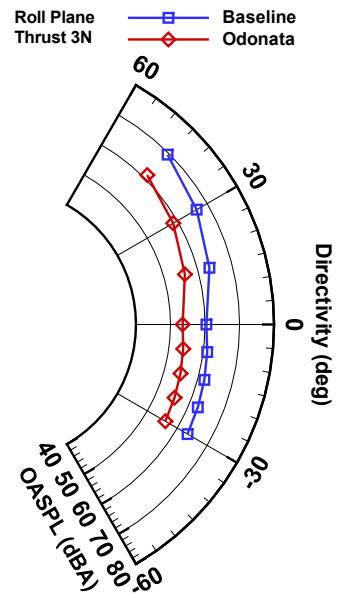
(c) Baseline and Hymenoptera roll plane directivity comparison



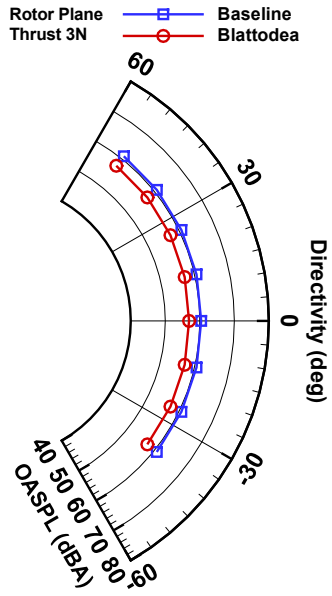
(d) Baseline and Maple Seed roll plane directivity comparison



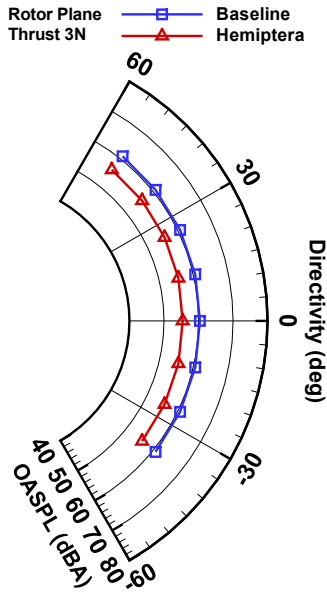
(e) Baseline and Neuroptera roll plane directivity comparison



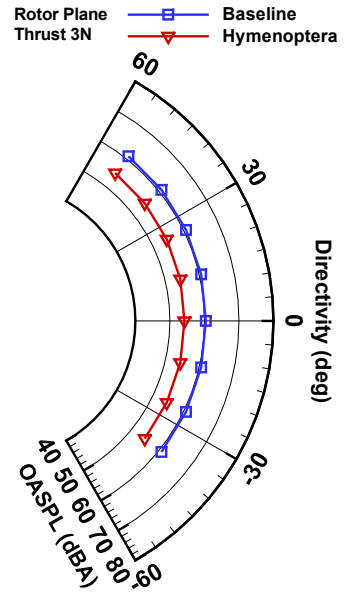
(f) Baseline and Odonata roll plane directivity comparison



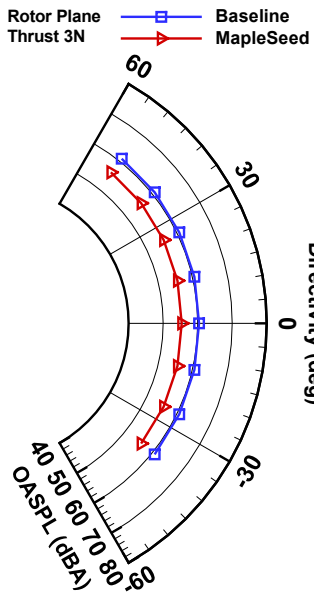
(g) Baseline and Blattodea rotor plane directivity comparison



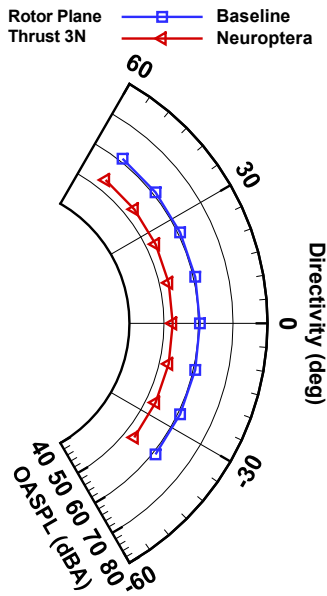
(h) Baseline and Hemiptera rotor plane directivity comparison



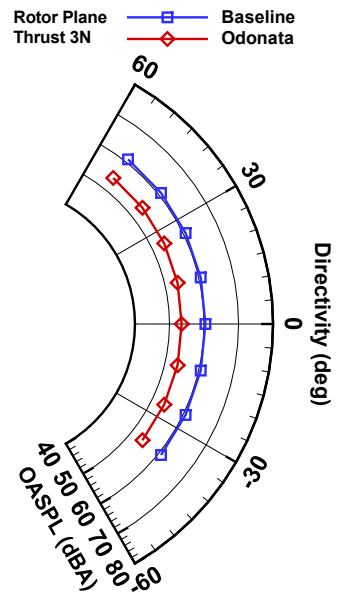
(i) Baseline and Hymenoptera rotor plane directivity comparison



(j) Baseline and Maple Seed rotor plane directivity comparison

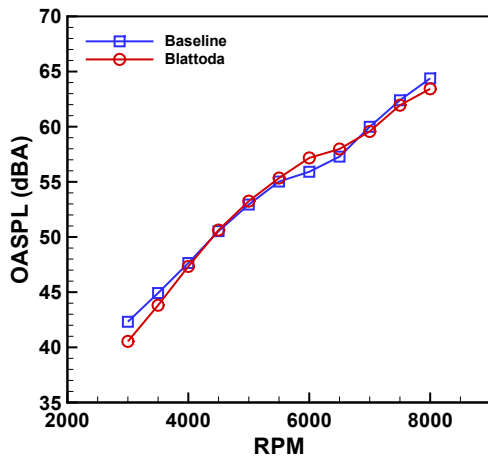


(k) Baseline and Neuroptera rotor plane directivity comparison

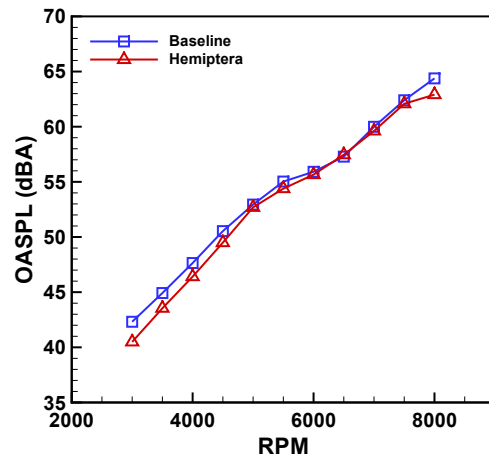


(l) Baseline and Odonata rotor plane directivity comparison

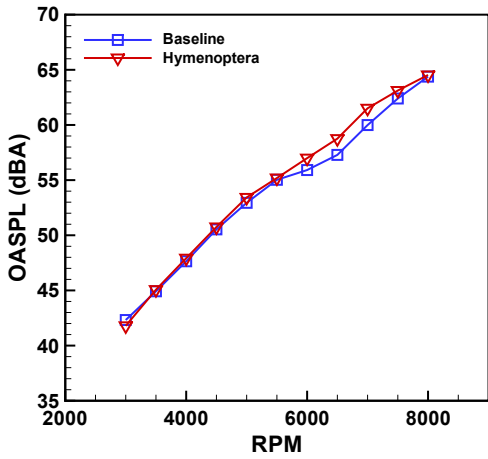
Fig. 8 Bioinspired propellers noise directivity at hover flight with 3N thrust compared to the baseline propeller



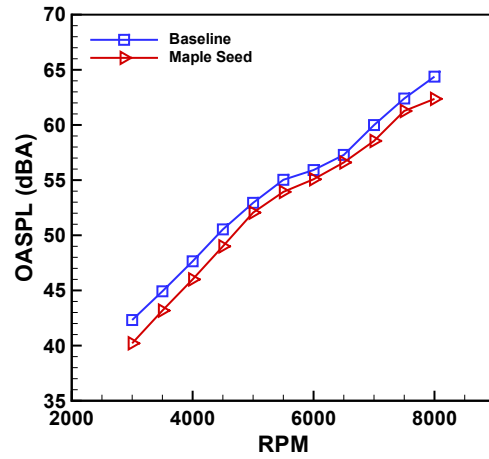
(a) OASPL of baseline and Blattodea propellers comparison in RPM



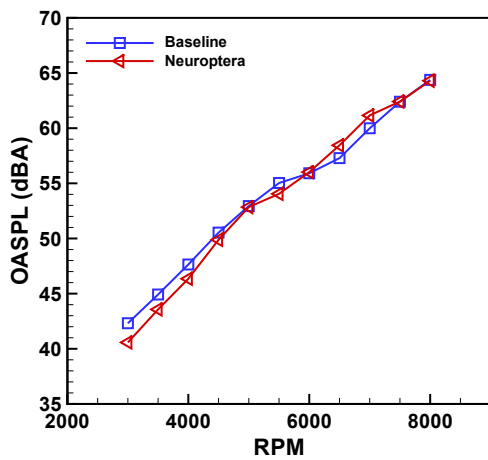
(b) OASPL of baseline and Hemiptera propellers comparison in RPM



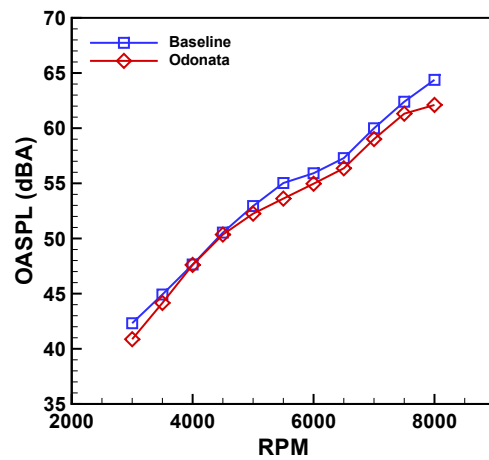
(c) OASPL of baseline and Hymenoptera propellers comparison in RPM



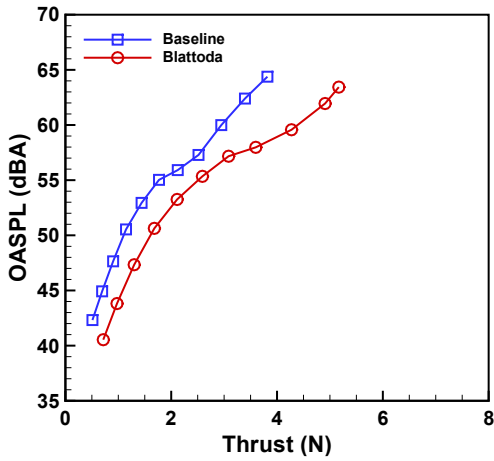
(d) OASPL of baseline and Maple Seed propellers comparison in RPM



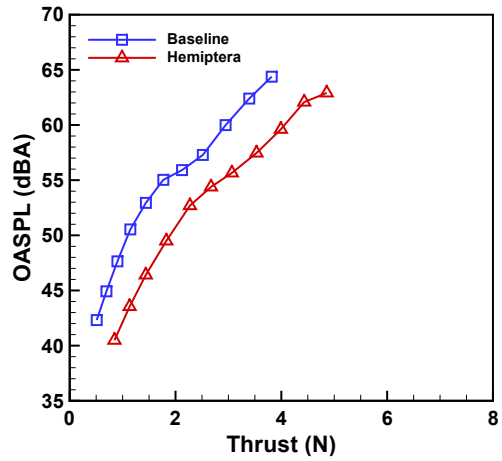
(e) OASPL of baseline and Neuroptera propellers comparison in RPM



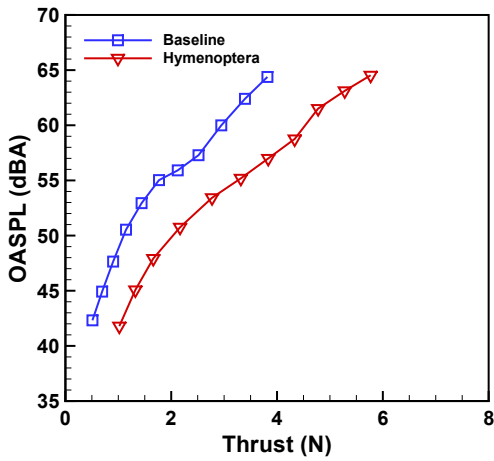
(f) OASPL of baseline and Odonata propellers comparison in RPM



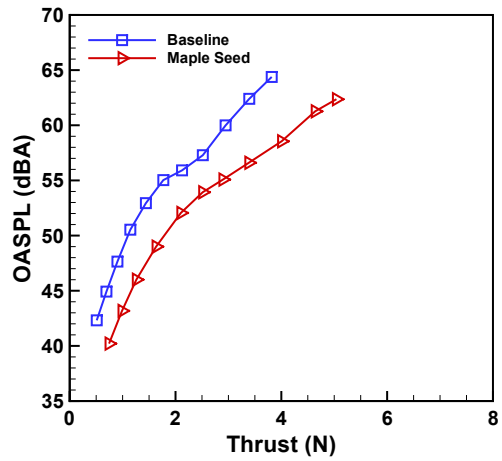
(g) OASPL of baseline and Blattodea propellers comparison in thrust



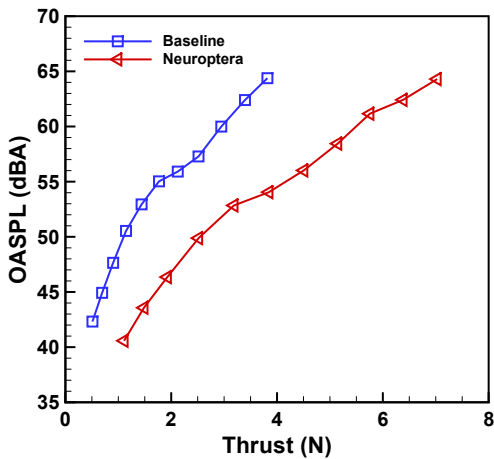
(h) OASPL of baseline and Hemiptera propellers comparison in thrust



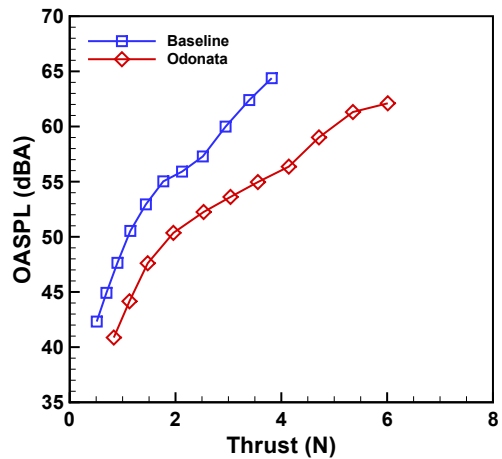
(i) OASPL of baseline and Hymenoptera propellers comparison in thrust



(j) OASPL of baseline and Maple Seed propellers comparison in thrust

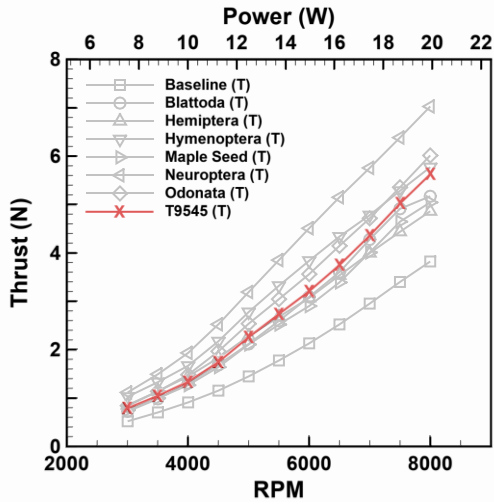


(k) OASPL of baseline and Neuroptera propellers comparison in thrust

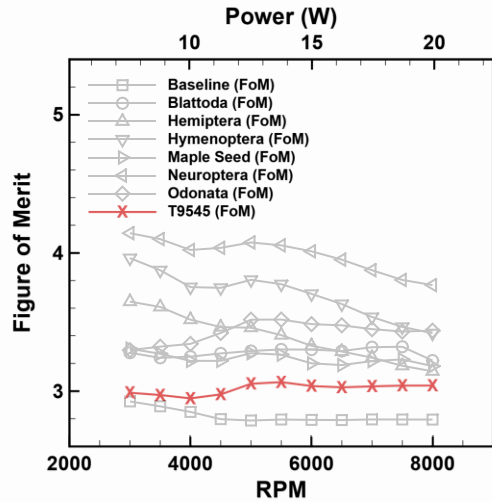


(l) OASPL of baseline and Odonata propellers comparison in thrust

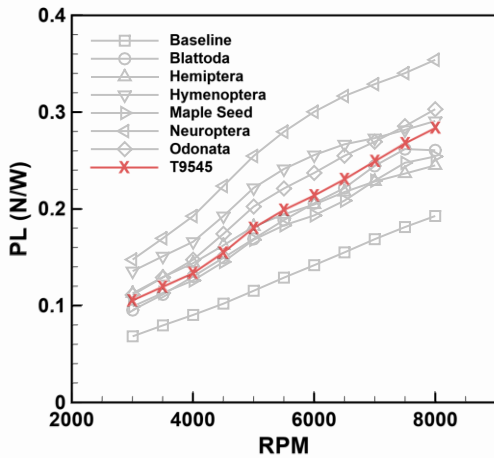
Fig. 9 Aeroacoustic performance results compared to the baseline propeller at microphone number five



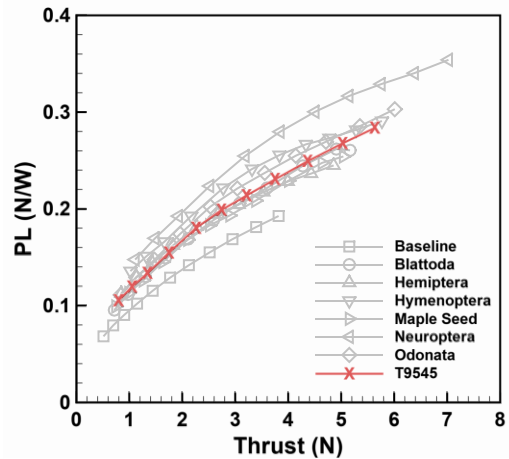
(a) Thrust of bioinspired propellers compared to the T9545 propeller



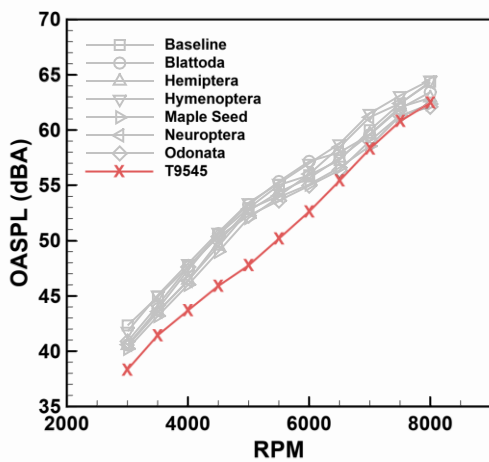
(b) Figure of merit of bioinspired propellers compared to the T9545 propeller



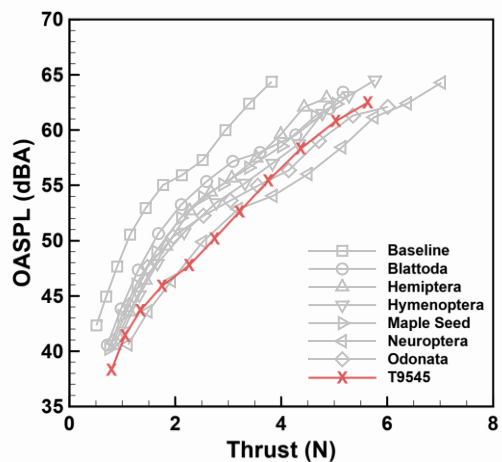
(c) Power loading of bioinspired and T9545 propellers comparison in RPM



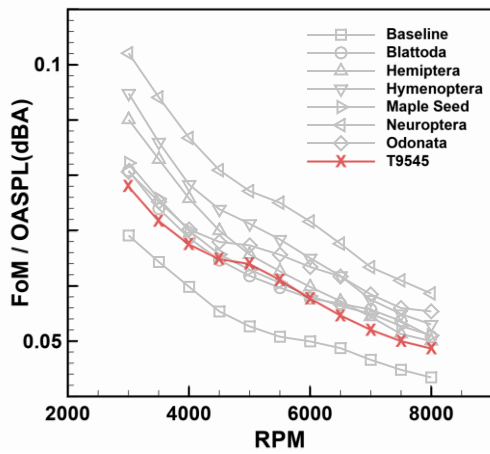
(d) Power loading of bioinspired and T9545 propellers comparison in Thrust



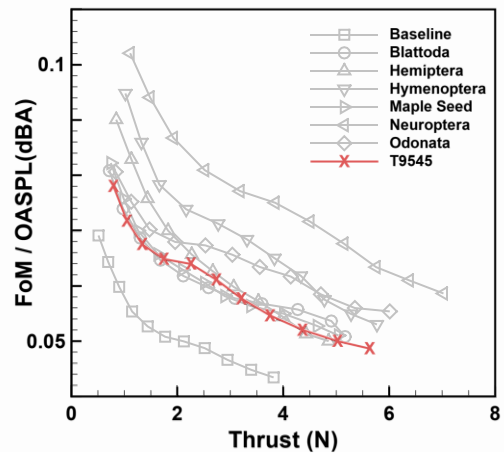
(e) OASPL of bioinspired and T9545 propellers comparison in RPM



(f) OASPL of bioinspired and T9545 propellers comparison in Thrust



(g) Aeroacoustic effect of bioinspired and T9545 propellers comparison in RPM



(h) Aeroacoustic effect of bioinspired and T9545 propellers comparison in Thrust

Fig. 10 Aerodynamic, Acoustic, and Aeroacoustic performance results of bioinspired propellers compared to the T9545 propeller at microphone number five

Table 1 Local chord-based Reynolds and Mach numbers of all propellers

1	0.9	0.8	0.7	0.6	0.5	0.4	0.3	0.2	0.1	r/R		Propeller
										RPM	Ma	
0.11	0.10	0.09	0.08	0.07	0.05	0.04	0.03	0.02	0.01	3000	3000	-
0.29	0.26	0.23	0.21	0.18	0.15	0.12	0.09	0.06	0.03	8000	8000	-
24962	29162	31524	32200	31493	29482	26269	21676	15113	5431	3000	3000	Baseline
11194	38423	44378	43463	38767	33382	27586	21558	13856	6100	3000	3000	Blattodea
9305	28790	37355	41384	40667	35594	26765	17399	9980	4196	3000	3000	Hemiptera
9937	34658	44043	46802	44560	35492	24614	16208	9371	4063	3000	3000	Hymenoptera
10306	27715	37235	41879	42203	37382	27758	17936	9996	4185	3000	3000	Maple Seed
8557	45101	53122	52425	45405	35932	26073	17534	10136	4210	3000	3000	Neuroptera
8709	39600	46809	45379	40566	34110	26132	18127	11012	4669	3000	3000	Odonata
66566	77764	84064	85868	83980	78618	70051	57803	40300	14482	8000	8000	Baseline
29850	102462	118342	115901	103380	89018	73561	57488	36949	16265	8000	8000	Blattodea
24814	76774	99612	110356	108446	94917	71373	46397	26614	11189	8000	8000	Hemiptera
26497	92421	117447	124804	118828	94645	65636	43222	24988	10836	8000	8000	Hymenoptera
27482	73908	99292	111676	112542	99685	74021	47828	26656	11159	8000	8000	Maple Seed
22819	120268	141658	139800	121080	95818	69528	46757	27030	11226	8000	8000	Neuroptera
23224	105601	124825	121010	108177	90959	69686	48340	29366	12452	8000	8000	Odonata